Title*:* Neural signatures of natural behavior in socializing macaques

Authors: Camille Testard†[1]*, Sébastien Tremblay†[1], Felipe Parodi[1], Ron W. DiTullio[1], Arianna Acevedo-Ithier[1], Kristin L. Gardiner[2], Konrad Kording[1,3], Michael L. Platt[1,4,5]

Affiliations:
[1]Department of Neuroscience, University of Pennsylvania, Philadelphia, PA, USA
[2]Department of Pathobiology, University of Pennsylvania, Philadelphia, PA, USA
[3]Department of Bioengineering, University of Pennsylvania, Philadelphia, PA, USA
[4]Department of Marketing, University of Pennsylvania, Philadelphia, PA, USA
[5]Department of Psychology, University of Pennsylvania, Philadelphia, PA, USA
†Co-first authorship
*Corresponding author. Email: camille.testard@pennmedicine.upenn.edu

Abstract
Our understanding of the neurobiology of primate behavior largely derives from artificial tasks in highly-controlled laboratory settings, overlooking most natural behaviors primate brains evolved to produce[1]. In particular, how primates navigate the multidimensional social relationships that structure daily life[2] and shape survival and reproductive success[3] remains largely unexplored at the single neuron level. Here, we combine ethological analysis with new wireless recording technologies to uncover neural signatures of natural behavior in unrestrained, socially interacting pairs of rhesus macaques within a larger colony. Population decoding of single neuron activity in prefrontal and temporal cortex unveiled robust encoding of 24 species-typical behaviors, which was strongly modulated by the presence and identity of surrounding monkeys. Male-female partners demonstrated near-perfect reciprocity in grooming, a key behavioral mechanism supporting friendships and alliances[2], and neural activity maintained a running account of these social investments. When confronted with an aggressive intruder, behavioral and neural population responses reflected empathy and were buffered by the presence of a partner. Surprisingly, neural signatures in prefrontal and temporal cortex were largely indistinguishable and irreducible to visual and motor contingencies. By employing an ethological approach to the study of primate neurobiology, we reveal a highly-distributed neurophysiological record of social dynamics, a potential computational foundation supporting communal life in primate societies, including our own.

MAIN TEXT

For long-lived social primates like humans, apes and monkeys, individual survival and reproductive success depend upon deft deployment of cooperation and competition, often by forming friendships and alliances that provide support in the face of social and environmental challenges[3–5]. In humans, social deficits severely impact daily life function for individuals with disorders like autism and schizophrenia, and the inability to connect with others is associated with depression and other long-term negative impacts on health and well-being[6–8]. Despite their importance, the neural circuit mechanisms supporting investments in long-term social relationships remain poorly understood, in part due to the challenges of recording neural activity or manipulating brain function during natural social interactions in humans and nonhuman primates alike.

For practical reasons, investigations of the neural basis of human and macaque social behavior have been restricted to highly-controlled laboratory settings in which individuals interact socially via an interposed computer, often in the context of economic games[9–16]. Despite the utility of this approach, which provides the opportunity to link neural signals to mathematically tractable variables, it neglects the natural behaviors primate brains evolved to produce and the social contexts that determine their function[1,17].

Here we focus on the neurobiology of dynamic social interactions in rhesus macaques (*Macaca mulatta*), a primate species closely related to humans whose behavior and biology has been better characterized than in any other primate species[18]. Moment-to-moment decisions to travel, forage, fight, groom, mate or rest in rhesus are strongly influenced by the presence, identity, and actions of other individuals[2,19]. Macaques form strong and stable bonds with specific individuals selected based on attributes such as kinship and social status[2]. These friendships and alliances, in part built and maintained through reciprocal grooming, enable mutual support to gain access to limited resources or fend off threats[20]. These observations imply that macaque brains encode rich information about the social environment, including identity, status, and kinship, as well as dynamic behavioral investments in social bonds through grooming and mutual support in response to threats, and integrate this information over multiple timescales to guide adaptive decision making.

Prior laboratory studies revealed a hierarchical organization of social information processing. From the perception of visual and auditory social cues in temporal cortex[21,22], to integration of others' actions, intentions and rewards in the orbitofrontal, cingulate, and prefrontal cortex[11,14,15,23]. Here, we build upon and extend these findings to identify how this system encodes information during unconstrained interactions between macaques with established social bonds. We focus on two areas located at two ends of the proposed social information-processing hierarchy. Area TEO in the inferotemporal cortex is part of the ventral visual stream[24], contains neurons that respond selectively to social cues like faces and body parts[21] and provides inputs to the "social interaction network"[23], including the ventrolateral prefrontal cortex (vlPFC). Neurons in vlPFC integrate multisensory social information[25], selectively respond to the visualization of social interactions[23], and contribute to context-specific goal-setting[26]. From this prior body of work, we predicted firing patterns of vlPFC neurons would contain rich information about individual behaviors, the presence and identity of neighboring monkeys, and reciprocal investments in relationships through mutual grooming and support in the face of threats. We also predicted social signals in vlPFC would be robust to visual orienting behavior and variation in movement kinematics which define behavioral states. By contrast, we predicted TEO neurons would preferentially encode visual social cues, be highly sensitive to changes in visual orientation and would not reflect current social and behavioral contexts.

To test these hypotheses, we developed new neural data-logging technologies to record from hundreds of single neurons in TEO and vlPFC in freely-moving, socially-interacting pairs of rhesus macaques within a larger colony. During hours-long sessions, we paired male subject monkeys with their female partners or isolated them, manipulated the identity of neighboring monkeys, introduced social stressors, and provided opportunities for the expression of macaques' natural behavioral repertoire, including non-social behaviors like foraging, locomotion, and rest. The extended duration of experimental sessions (~2.5hrs) allowed monkeys to engage in iterated grooming interactions and achieve reciprocity over multiple timescales, from minutes to hours or even days. Combining ethological, computer-vision and neural population analytical methods, we discovered widespread, robust neural signatures, in both brain areas, of 24 natural behaviors and their social context, which were not reducible to sensorimotor contingencies. Neural responses indexed social support and empathy in response to an

external stressor. Remarkably, neurons in both brain areas tracked dynamic investments in grooming given and received to achieve and maintain the reciprocity necessary to support long-term social bonds. Together, our findings reveal a highly-distributed neurophysiological ledger of social dynamics unfolding across multiple contexts and extended timescales, which is capable of supporting the affiliative bonds that drive survival and reproductive success in gregarious primates including humans.

Unrestrained macaques recapitulated their natural behavioral repertoire

Subjects were two male rhesus macaques interacting spontaneously with their respective female partners over 2.5-hour long sessions in their home enclosure (N = 12 sessions, 6 per subject; **Fig 1A**). In each session, we provided monkeys with foods requiring manual extraction from a turf board (i.e. foraging) and experimentally manipulated social context pseudo-randomly in a block design by: 1) isolating or pairing the subject with his female partner, and 2) when paired, varying the identity of neighboring monkeys (total: 3 conditions; **Fig 1A**). Neighbors were monkeys in the adjacent enclosure that were visible but not physically accessible. The behaviors we focused on occurred over seconds to minutes and were labeled manually from videos captured by 7 cameras, at the second resolution, by two primatologists with extensive field experience (96% inter-rater reliability, see **Methods**) using a well-validated ethogram derived from observations of free-ranging rhesus macaques (**Appendix 1-2**).

Monkeys exhibited a variety of aggressive, affiliative, locomotive, and feeding behaviors typical of rhesus macaques, and recapitulated most of their natural behavioral repertoire observed in the wild (N=24 observed behaviors; 84% overlap with wild macaque ethogram, **Fig 1B-C**). While paired, monkeys spent most of their time grooming (>60%, **Fig 1C**), defined as repetitively brushing another monkey's fur. In macaques, like other primates, grooming serves as an investment that builds and maintains strong social bonds (i.e., friendships). Male-female pairs showed remarkable short and long-term reciprocity in grooming in our study (see **Fig 4** below). Aggression constituted a small but significant portion of social interactions (9%) and was most frequently expressed in response to threats from human intruders (see **Fig 5** below). Rest, defined as sitting and observing the environment passively without engaging in any other overt actions, occurred 33% of time.

Transitions from one behavior to another were highly-structured, with some behaviors followed by specific behaviors with high probability (**Fig 1D, S1A**). For example, a monkey soliciting another monkey to groom himself elicited a grooming bout with 68% probability, whereas a subject monkey being threatened provoked an aggressive response with 60% probability. Behavioral transitions coalesced into affiliative (left) and aggressive clusters (right; **Fig 1D**), establishing two major affective contexts for behavior.

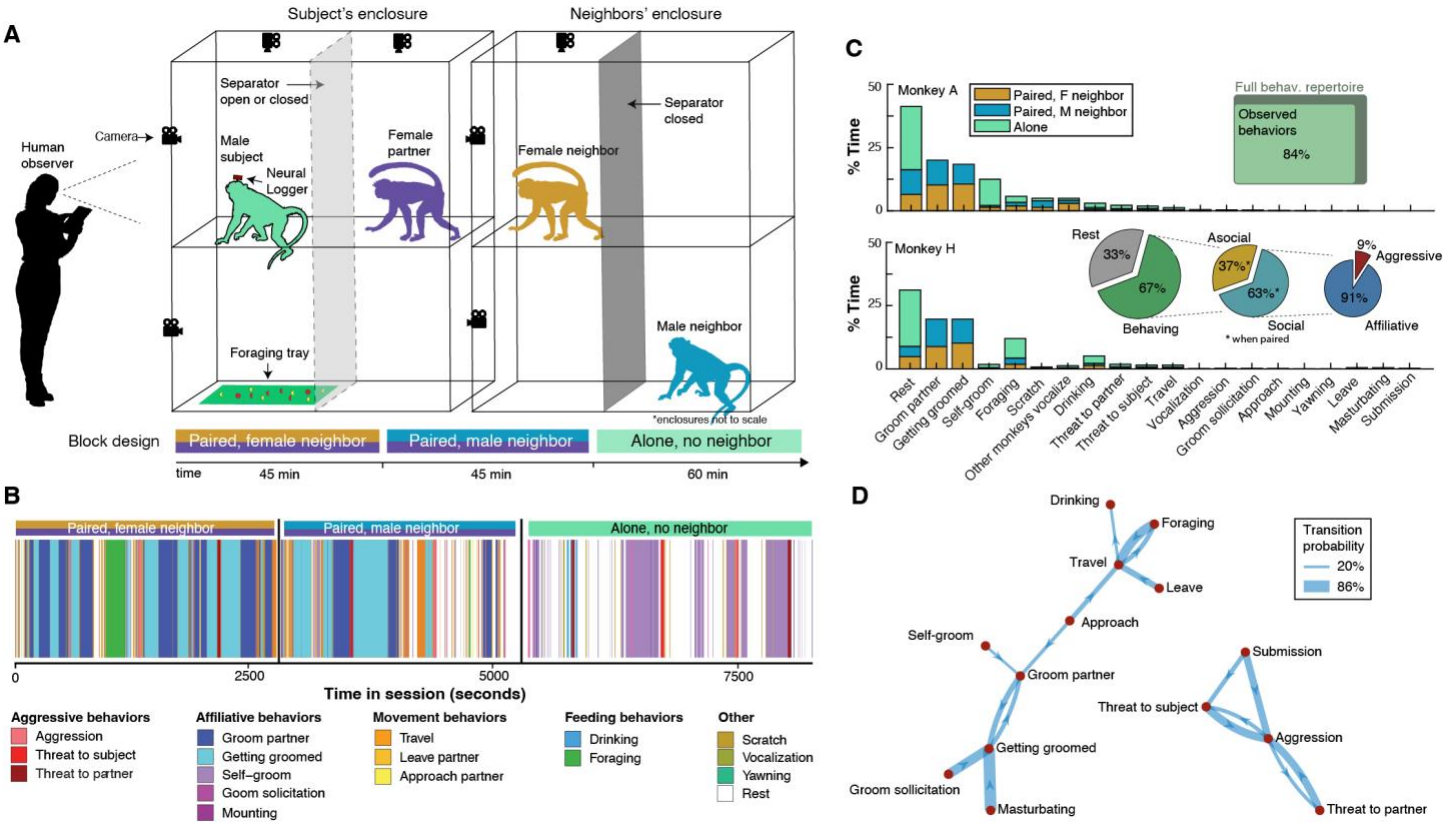

Fig 1. **Unrestrained socially-interacting macaques spontaneously express their species-typical behavioral repertoire.** (**A**) Experimental setup with two male-female pairs in adjacent enclosures. Neural activity was recorded from male subjects during various social contexts and behaviors in 2.5-hour sessions (N=6 sessions per male subject, N=2 male subjects). (**B**) Species-typical behaviors expressed during 3 social contexts over the course of a typical recording session (N=24 behaviors over 12 sessions). (**C**) Proportion of time engaged in each behavior across all 12 sessions, for each male monkey. When paired, monkeys engaged in social behaviors with their partner 63% of the time. (**D**) Behavioral state transition probabilities (thresholded >20%) segregate into affiliative (left) and aggressive (right) clusters (see **Fig S1A** for full behavioral transition matrix). Monkey and human silhouettes in (A) created with BioRender.

Single neuron activity is broadly modulated by species-typical behaviors

We developed and deployed new technology that interfaced chronically-implanted, multi-electrode Utah arrays (Blackrock Neurotech, UT) with miniaturized, wireless data-loggers (Deuteron Technologies, Israel) to record from approximately 300 single neurons (single and multi-units) per session (**Fig 2A**, mean = 307.42 units, SD = 19.67) while monkeys moved and interacted freely in their home environments (**Movie S1-4**). This technology allowed us to obtain stable, high-quality neuronal action potential recordings with unlimited spatial range, while minimizing the footprint of cranial implants (see **Fig S1B-C**). We analyzed firing rates of individual neural units in 1 sec bins to match the timescale of behavioral quantification (see **Methods**). We compared the firing activity of neurons during different behavioral states to activity during a reference state of "rest", as defined above.

Over the course of a session, single neuron activity in both TEO and vlPFC showed striking modulation as a function of behavioral state (**Fig 2B, S2A**), some of which deviated strongly from firing rates during rest (**Fig 2C**). We quantified these deviations from rest using an effect size metric comparing the means of the two firing rate distributions (Cohen's d). In a "Neuro-ethogram" plot, we depicted the differences in mean firing rates between each behavioral state and rest (i.e., effect size) across an example population of simultaneously recorded

neurons (**Fig 2D**). Single neurons collectively decreased firing rates during affiliative behaviors and increased firing rates during aggression-related behaviors, traveling, and foraging (**Fig 2E**). Surprisingly, patterns of neuronal modulation in TEO and vlPFC as a function of behavior were largely indistinguishable (except for foraging in certain sessions). Despite TEO long being considered a core component of extrastriate visual cortex based on anatomical connections and neurophysiological responses[27–29], neuronal activity clearly carried information about the behavioral state of the animal (example TEO unit in **Fig 2B**), even as visual fields varied substantially within a behavior and overlapped with visual fields occurring in other behavioral states (see **Fig 6** below for detailed visuomotor analyses).

Across both brain areas, the firing rates of most neurons were significantly modulated by a large array of natural behaviors (median = 7.2 behaviors, **Fig 2F**; see statistically thresholded neuro-ethogram in **Fig S2B**) rather than being modulated by a few specific ones—a finding that held even when restricting our analyses to well-isolated single units and controlling for sample size (**Fig S2C-D**). Although concurrent selectivity for 2-3 task variables (i.e. mixed selectivity) has been reported in many laboratory tasks[30–32], the level of mixing we observed during natural behavior exceeds previous reports in controlled laboratory environments[33,34] (**Table S1**), and supports a distributed rather than sparse coding model of cortical activity in primates. Theories proposing sparse coding as a mechanism by which the brain balances metabolic constraints with information-processing capacity[35,36] may need reconsideration in light of these observations. Perhaps "coding through neural inhibition", as observed for many affiliative behaviors in this study (**Fig 2D-E**; left side), is key to reconcile metabolic constraints[37] with the distributed coding we observed.

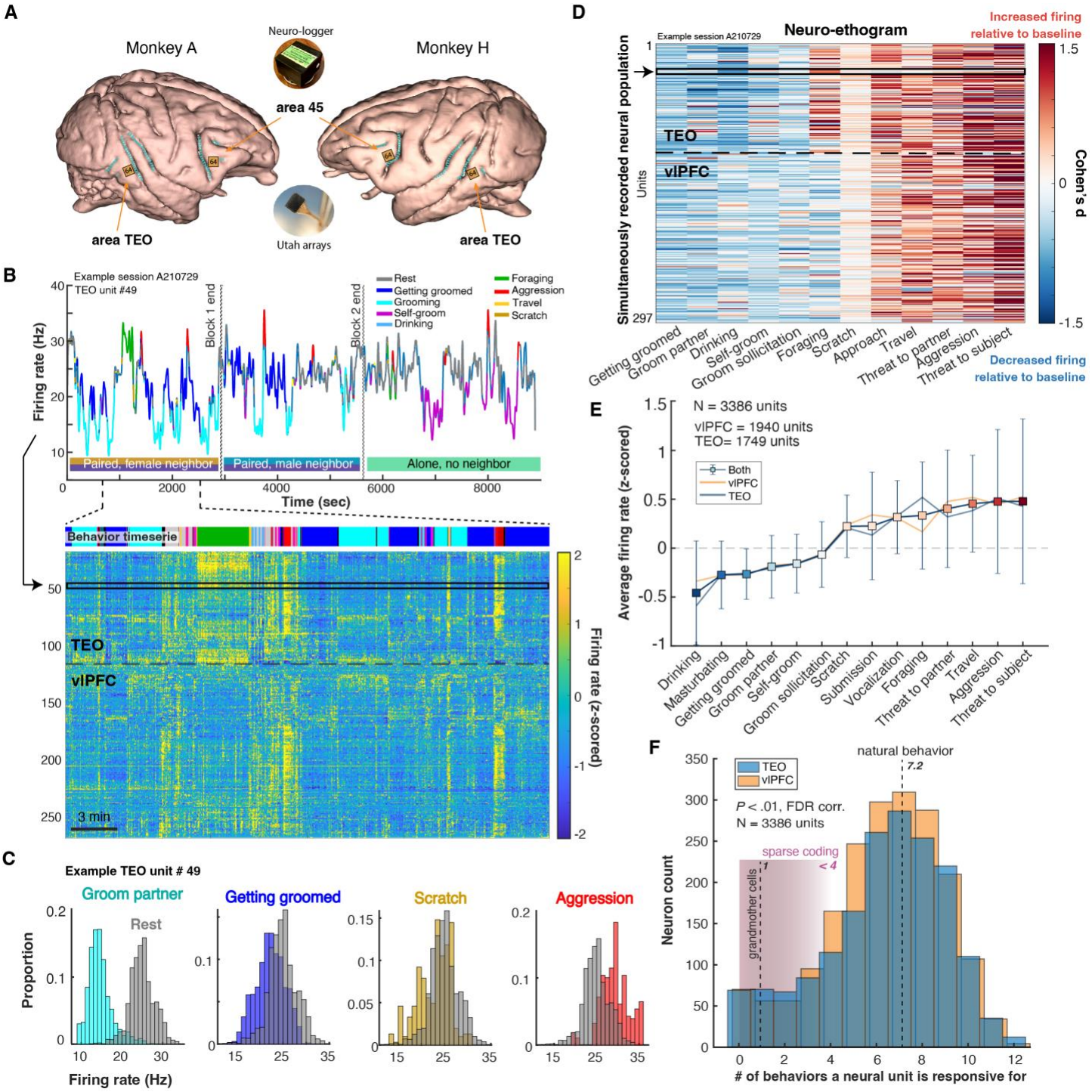

Fig 2. Single neuron activity varies across the natural behavioral repertoire. (**A**) 3D MRI-based reconstruction of male subjects' brains and neural recording locations. Two 64-channel Utah arrays were implanted in the right hemisphere for monkey A and left hemisphere for monkey H. Data was stored on a wearable microSD card using a data-logger (inset). (**B**) Top panel: Example TEO unit firing rate trace (smoothed for visualization) during an example 2.5-hour session with the subject's behavior labeled. Bottom panel: Z-scored firing rate over the entire population of simultaneously recorded units for ~33min of the session (See **Fig S2A** for full session), y-axis ordered with hierarchical clustering. Example unit from top panel shown with black arrow. (**C**) Normalized histograms of the distribution of firing rates during a particular behavior compared to 'rest' (reference behavior; gray) for the same example unit as in B. (**D**) Neuro-ethogram plot displaying effect sizes (Cohen's d) of difference in distributions of firing rate during each behavior (columns) which occurred for at least 30 sec in the session compared to rest (as in C), for all units (rows), during an example session. Example unit from panels B

and C shown with a black arrow. Red: excitatory responses; Blue: inhibitory. See **Fig S2B** for a statistically thresholded neuro-ethogram. (**E**) Averaged z-scored firing rates of all TEO and vlPFC units as a function of behavior, pooled across monkeys. Behaviors are ordered from low to high average firing rate. Error bars represent standard deviations. (**F**) Distribution of the number of behaviors for which each neuron was responsive (*t*-test, FDR-corrected, $P < 0.01$), separated by region of interest, pooling across animals. The sparse coding theory (pink shading) would expect each neuron to encode < 4 behaviors (**Table S1**). "Grandmother cell hypothesis" would predict selectivity to a single behavior.

Behaviors and social contexts structure neural population activity

We next examined activity across the population of simultaneously recorded neurons, which can reveal information not detectable in the average activity of individual neurons[38,39]. We applied multivariate analytical methods to investigate neural signatures of the diversity of natural behaviors and their variation across social contexts in vlPFC and TEO population activity. First, we visualized neural population activity patterns using an unsupervised nonlinear dimensionality-reduction technique, *Uniform Manifold Approximation and Projection* (UMAP) [40]. Nearby points in this dimensionality-reduced space represent similar neural states and this visualization provides insights into how neural states are structured as a function of behavior and social context.

When plotting the first 3 UMAP axes, we observed that neural population activity in vlPFC spontaneously clustered along species-typical behavioral states such as grooming, foraging and aggression (**Fig 3A,** see **Fig S3A-B** for plots including all behaviors). Surprisingly, neural activity in TEO also spontaneously clustered along behavioral states (**Fig 3B**). Neural population signatures of behavior in both vlPFC and TEO were not reducible to potential visual confounds associated with each behavior (see **Fig 6** below). Patterns that were not obvious from analyzing the activity of individual units emerged clearly when considering population activity. For example, grooming and being groomed were both associated with suppression of mean firing rates of individual units (see **Fig 2D**), but segregated into distinct clusters when the simultaneous activity of all recorded units was considered (**Fig 3A,B**).

Importantly, we identified that population state clusters for most behaviors were divided into sub-clusters. For example, the clusters 'Groom partner' and 'Getting Groomed' (black arrows in **Fig 3A,B**) are split into two sub-clusters, both in area vlPFC and TEO. When we recolored each UMAP plot according to social context instead of behavior, we found these subclusters were explained by the social context in which those behaviors were performed(**Fig 3C,D**). For example, the cluster 'Groom partner' (black arrows in **Fig 3B**) split into two sub-clusters which correspond to whether the neighbor was a male or a female during the grooming bout (black arrows in **Fig 3C** indicate the same sub-clusters). Thus, the structure of neural population activity also reflected the social context in which behaviors occurred. Simultaneous representation of both actions and contexts may be a mechanism by which neural activity tracks and guides context-dependent behavioral choices in socially-interacting primates.

To complement UMAP visualizations of the data, we applied a widely used linear decoding technique (Support Vector Machine[41], see **Methods**) to determine what information a hypothetical downstream brain region could decipher from neural activity in TEO and vlPFC. Natural behaviors were highly decodable on a moment-by-moment basis from the simultaneously recorded neural activity of both brain areas, together and from each independently (mean decoding accuracy 84%, N=12 behaviors with >30 samples per session, **Fig 3E**). Remarkably, we found that social context was also linearly decodable (mean accuracy >80%, **Fig 3F**) from one or both brain areas during various behaviors. It was possible, for example, to decode whether the subject monkey was foraging alone or with his partner, or whether the neighboring monkey was a male or a female during a bout of aggression. Together, these findings resonate with decades of field observations of primates demonstrating the

importance of social context, such as the identity of neighboring monkeys, in the decision-making processes that drive behaviors like socializing, foraging, or traveling[42,43].

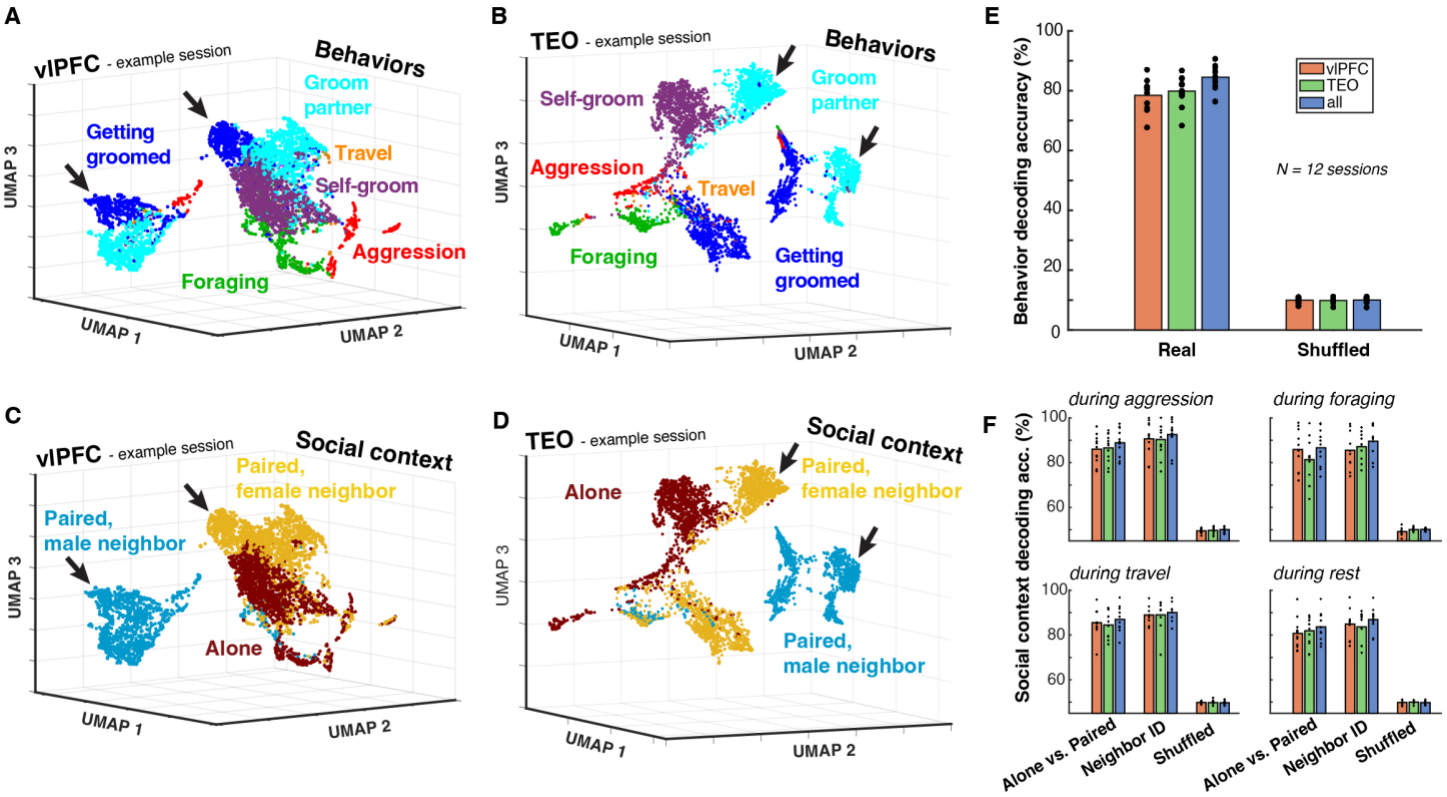

Fig 3. **Neural population activity simultaneously encodes current behavior and social context.** (**A**) Neural population states in one example session visualized using unsupervised UMAP, color-coded post-hoc by subject's behavior. Each point represents simultaneous firing of all vlPFC (A) or TEO (B) units for a 1 second bin. For ease of visualization, only behaviors that occurred for at least 30 sec within a session are plotted and "rest" is excluded (see **Fig S3 A-B** for a plot including all behaviors, **S3C-D** for Euclidean distances within and between behavior states & contexts in UMAP space across all sessions, and **S3E-H** for UMAP projections using different parameters). (**C-D**): Same neural space as in A-B but now color-coded by social context (i.e., alone, paired & female neighbor, paired & male neighbor). Black arrows point to example behavioral sub-clusters that segregate according to context (**E**) Decoding accuracy for the behavioral ethogram across sessions, only considering behaviors which occurred at least 30 seconds in a session (mean N= 12 behaviors on any given session, chance = ~8%). Each dot represents a session. (**F**) Decoding social context during aggression, foraging, travel and rest separately. Chance is ~50%, same color-code as in E.

Neural population activity tracks grooming reciprocity

Strong, stable relationships in humans and other animals are maintained through reciprocal interactions[44]. In macaques and other primates, reciprocity takes the form of mutual grooming or support in the face of challenges[20] and can occur over days to months[45,46]. It has been proposed that an internal "mental account" tracks these mutual social investments over long periods of time ("calculated reciprocity"[47]). We next investigated the behavioral and neural mechanisms supporting grooming reciprocity over time in the two male-female pairs.

Combining grooming interactions across all chronologically consecutive sessions, both male-female pairs showed remarkable reciprocity in both the number of grooming bouts and total duration of grooming (**Fig 4A,B**). The observed level of reciprocity in bout quantity (>0.96 in both subjects, 1=perfect reciprocity and 0=fully one-sided, see **Methods**) was highly unlikely to occur by chance (P < 0.0001 for both pairs, **Fig 4C** top panel). Subject

monkeys took turns grooming (i.e., alternated in quick succession, $P < 0.001$ for both pairs, **Fig 4C** middle panel, **Fig S4A**), which can facilitate tracking the number of bouts to achieve reciprocity, but did so in less than 50% of grooming interactions. These findings thus suggest monkeys tracked the number of bouts given and received over longer time intervals to achieve observed levels of reciprocity.

Monkeys also tracked grooming duration. The observed near-perfect grooming duration reciprocity (>0.98) would be unlikely to occur by chance ($P < 0.05$ across both monkeys, **Fig 4C** bottom panel). One simple heuristic to achieve equal duration is to match the length of the immediately-preceding grooming bout. We did not find a correlation between the durations of consecutive alternating grooming bouts (r=0.04, p>0.7, **Fig 4D**), suggesting monkeys did not use this heuristic. Instead, reciprocity was progressively achieved over the course of the study, both within 2.5 hour-long sessions (**Fig 4E**) and across multiple days (**Fig 2B**). Remarkably, small grooming duration imbalances at the end of one session were rebalanced in subsequent sessions, which could occur up to 7 days later (**Fig 4F**). Taken together, these observations suggest that monkeys maintain a running "mental account" of both the quantity and duration of grooming bouts given and received, over extended periods of time, to achieve reciprocity. This exceptional cognitive competence has not been previously documented in monkeys with the temporal resolution afforded by our study and, in this context, supports "calculated reciprocity"[47,48].

We investigated potential neural signatures of this mental accounting by asking whether and how population activity in TEO and vlPFC tracked net number of grooming bouts and grooming duration (Net = Receive - Give, **Fig 4A**). We also investigated neural tracking of elapsed time within a session since it was, in some sessions, correlated with net groom time. We used multi-linear ridge regression analysis with 5-fold cross-validation to predict these 3 continuous variables from neural population activity (**Fig 4G**, see **Methods**). We found that population activity in both brain areas and both monkeys predicted net number of bouts and net grooming duration within a session (mean R^2 net duration = 0.16, R^2 net bout number = 0.47, **Fig 4H-I**, **S4C-D**). Model predictions for net grooming duration, however, were much weaker than for net number of bouts and could be explained by elapsed time within a session (**Fig S4E,F**). Net grooming bout, on the other hand, did not correlate with time and was also highly decodable from neural population activity (>80% accuracy, **Fig S4E,F**). We therefore hypothesized that long-term mental accounting for grooming reciprocity occurs by integrating elapsed time with net number of bouts given vs. received, rather than tracking net time spent grooming. No single neuron on its own could predict these reciprocity metrics as well as the entire neural population (**Fig S4G**). Moreover, the distribution of single neuron model fits were indistinguishable across all three models (duration, bout and time), even though they significantly differed when considering the neural population as a whole (**Fig 4H-I**, **S4G)**. These findings suggest that a highly distributed neural code supports mental accounting of grooming bouts and elapsed time in order to achieve reciprocity.

Notably, neural tracking of elapsed time was stronger when monkeys were grooming than when they were not (**Fig 4J**). UMAP visualizations of neural activity during grooming showed striking temporal structure defined by bout number, whereas UMAP visualizations of neural activity during rest were not temporally structured to the same extent (**Fig 4K**). This difference was also reflected in higher linear decoding performance for chronological bout number during grooming compared to rest (mean accuracy during grooming: 89%; rest: 59%; chance: 10%, **Fig S4F**). This result endorses the hypothesis that grooming, which is both rewarding and holds unique functional significance for building and maintaining relationships, enhances the salience and importance of elapsed time. Overall, our findings reveal a potential neural mechanism by which reciprocity is tracked in social relationships, and failures of this mechanism could lead to pathological social behavior, from egoistic personalities to psychopathy.

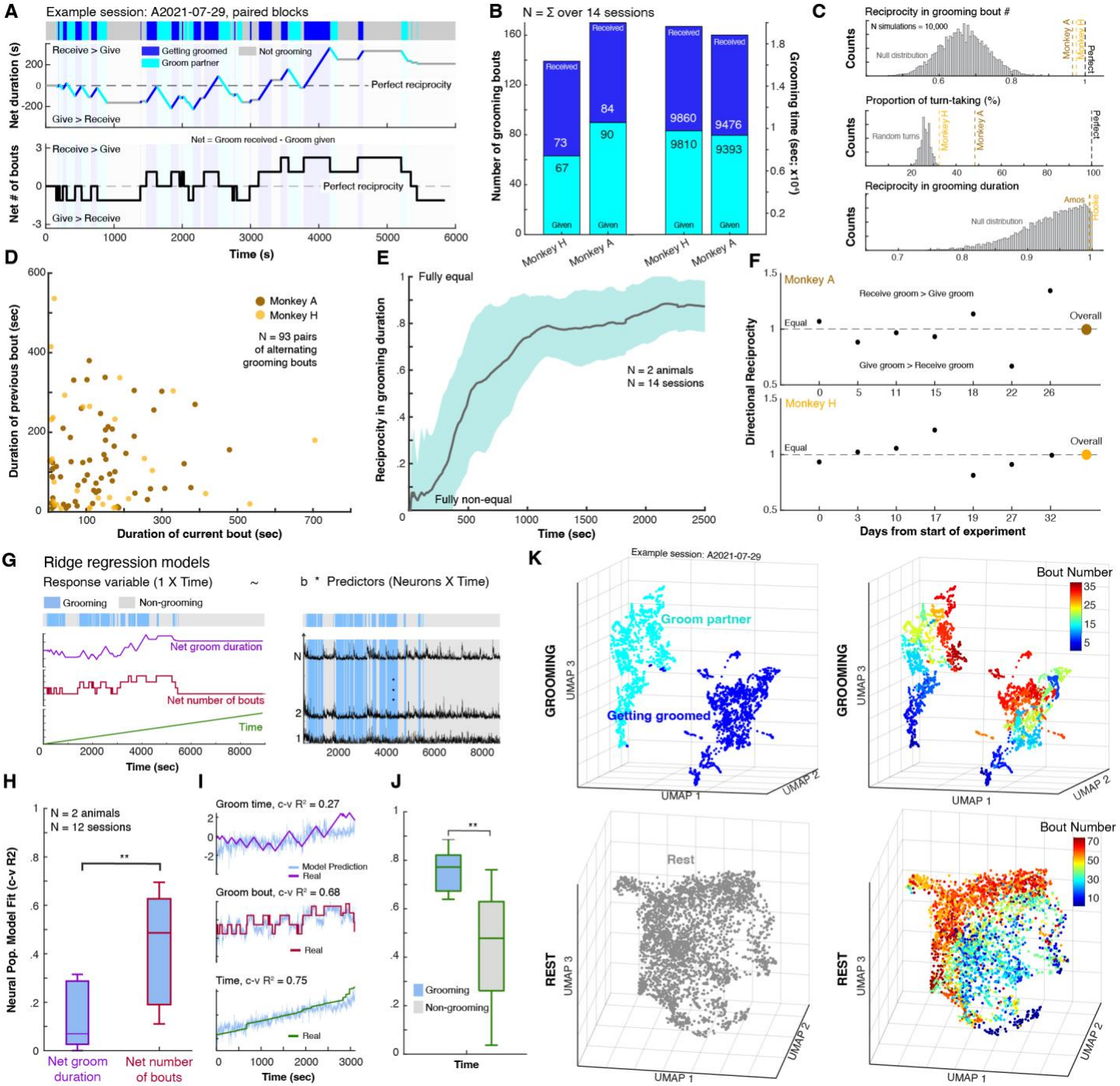

Fig 4. **Neural population activity tracks reciprocity in socializing macaques** (**A**) Reciprocal grooming for an example session. Top: grooming bouts over time, received (dark blue) or given (cyan). All non-grooming behaviors are lumped into a "not grooming" category (gray). Middle: Net grooming duration in seconds in the session. Bottom: Net number of grooming bouts in the session. Net = Received - Given. Dashed lines indicate perfect reciprocity (**B**) Number of grooming bouts (left) and grooming time (right) given (cyan) and received (dark blue), for both subject pairs, summed across all sessions. (**C**) Simulations assuming monkeys were grooming randomly. 1 = perfectly reciprocal, 0 = fully one-sided. Simulations were run 10,000 times to obtain likelihood of the observed reciprocity if monkeys were not intentionally trying to reciprocate number of bouts (top), engage in turn-taking (middle) or reciprocate grooming duration (bottom) (see **Methods**). (**D**) Correlation in duration of consecutive alternating grooming bouts (e.g. I groom you, then you groom me). (**E**) Mean reciprocity in grooming duration over time during a session, averaged across sessions. Shaded area represents standard errors. (**F**) Directional reciprocity (y-axis) across sessions which were separated by multiple days (x-axis).

Directional reciprocity goes from 0 to 2, with 1 being equal grooming duration, <1 more groom given than received, >1 more groom received than given (see **Methods**). (**G**) Schematic of ridge regression approach to predict net grooming duration, net number of bouts and time elapsed within a session from the neural population activity. (**H**) Cross-validated model fit (R^2) for net duration and net number of bouts models using ridge regression. Predictions based on neural activity during grooming only. (**I**) Model predictions and real values for net grooming duration (top), net number of bouts (middle) and time elapsed (bottom) for the same example session as in (A). (**J**) Cross-validated model fit (R^2) for predicting time elapsed during grooming and outside of grooming. (**K**) Unsupervised UMAP projection of neural population activity during grooming only (top) vs. rest only (bottom), pooled across both brain areas. Left: neural states in UMAP space color-coded by behavior. Right: color-coded by chronological bout number in this session. Bout numbering in grooming includes both directions (give and receive). Note that 14 sessions were used for panels A-F and 12 sessions for panels H & K. We included 2 additional sessions for behavioral analyses in panels A-F which did not include neural data to portray all consecutive sessions we recorded in this experiment, which was critical to unveil the temporal dynamics of reciprocity over multiple days.

Neural responses to threats reflect empathy and social support

Social relationships help primates cope with external stressors, such as environmental disruption[5] or aggressive encounters with conspecifics[49]. Social support is associated with lower physiological response to threats in the presence of a supporting partner. One important emotional driver of this social support is empathy– emotional resonance with the feelings of a partner. Here, we investigated the neural correlates of both social support and empathy using a standard "human intruder" paradigm designed to elicit aversive responses (**Fig 5A**). We analyzed behavioral and neural responses to 30 seconds of open-mouth threats (a particularly aversive stimulus for macaques[50]) directed towards the subject monkey or his partner, while the subject was either alone or paired.

Open-mouth threats provoked aversive reactions by our subjects, including aggressive displays, attacks, and submissions, which we combined into an "agitation" score. We found that agitation was strongest when subjects were alone, and the presence of a partner reduced agitation by 27% (**Fig 5B**, two-sample t-test; $t(1, 36) = 2.9$, $P = .006$, see **Fig S5A** for results separated by monkey). Similarly, neural responses to threats were dampened when subjects were paired with a female partner, as measured by the Euclidean distance in UMAP neural space relative to baseline (**Fig 5C,** $P < .01$, see **Fig S5B** for results separated by monkey). Remarkably, female partners consistently groomed their male partner following threats, consistent with the known stress-reducing functions of this affiliative behavior (**Fig S5C**). When the subject and the partner were paired, threats directed towards the partner elicited aversive defensive reactions from the subject, albeit to a lesser extent than threats directed to himself (**Fig 5B-C**). Threats towards the subject or his partner elicited remarkably similar patterns of neural population activity (**Fig 5D,** representational similarity of $r = 0.91$ for monkey A and $r = 0.90$ for monkey H). The similarity of neural responses to threats directed towards oneself and towards the partner may be a correlate of social empathy experienced by individuals who witness their partner under stress. This population-level mirroring of the emotional response may be critical in motivating a defensive reaction to support the other, a support which buffered both behavioral and neural responses to threats in our subjects.

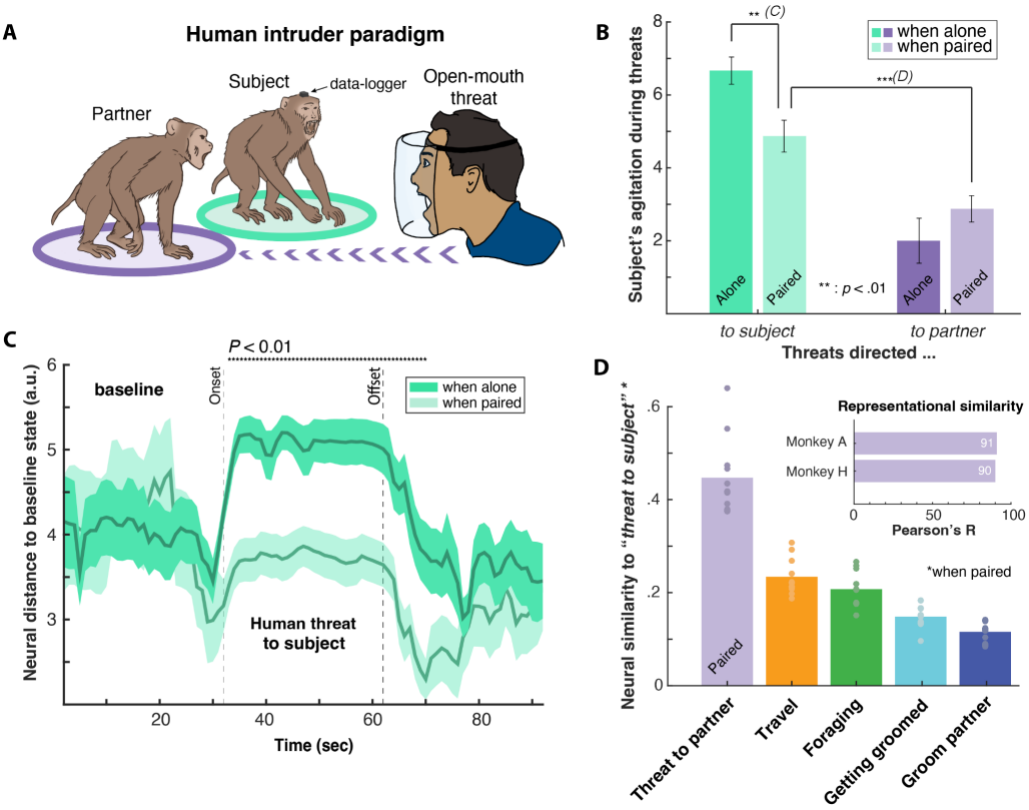

Figure 5. Behavioral and neural evidence for social support and empathy in response to threats. (**A**) Schematic of the "human intruder" paradigm (see Methods) where, in this example, the partner is being threatened by an experimenter with an open-mouth threat for 30 seconds. Both the partner and subject monkeys were threatened while alone, or with a partner (**B**) Behavioral responses to human threats towards the subject or the partner, when alone (dark bars) or paired (light bars). Agitation measured by manual scoring of videos (details in Methods). (**C**) Mean Euclidean distance from baseline (center of mass of 'rest' states) in UMAP neural space during threats towards the subject in the alone (dark green) vs. paired conditions (light green), averaged across threat bouts (N = 25 alone, N = 24 with a partner). Shaded areas represent SEM. (**D**) Similarity score in UMAP space between the subject's neural states during threat to subject and threat to partner (purple), and other reference behaviors. Each circle corresponds to the mean similarity score for one session. Inset: Representational similarity analysis showing the correlation coefficient between the average neural population responses during threat to subject compared to threat to its partner while paired. Artwork in (A) by Jordan Matelsky.

The effects of free movements and gaze direction on neural signatures of natural behavior

Movements dominate cortical dynamics in mice[51,52] and explain a large portion of neural activity in macaque cortex during laboratory tasks[53]. Moreover, area TEO has long been linked to visual processing of objects and social stimuli[24]. These observations raise the question of whether the patterns of neural population activity we uncovered reflect movements or visual inputs associated with specific behaviors and social contexts rather than the behaviors or contexts themselves. To address this possibility, we quantified movements and field of view from video using deep learning approaches (**Fig 6A**, see **Methods**) and related these measurements to neural activity using complementary analytical methods.

It is not possible to entirely decorrelate behaviors from movements since behaviors are defined, in part, by movement patterns. We can, however, examine times when similar movements were performed during different behaviors and in different contexts. For example, similar visually-guided reaching and facial movements were performed during "self-grooming" or "grooming a partner" (**Fig 6B**). It was nonetheless possible to linearly separate the neural representations of these two behaviors (**Fig 3E**), which would not be possible if movement kinematics solely defined these neural signatures. We found that each behavior was characterized by a wide

distribution of head orientations, encompassing distinct fields of view and, thus, visual inputs during the execution of a given behavior (**Fig 6C**). The invariant behavioral decoding accuracy amidst changing visual inputs suggests robustness of the underlying neural representations of behavior. Moreover, similar distributions of fields of view occurred during multiple distinct behavioral states (>50% overlap), further dissociating visual inputs from neural coding of behavioral states (**Fig 6C**). Similarly, fields of view largely overlapped (75% overlap) across different social contexts (**Fig 6D)**, yet social contexts were still decoded accurately (see **Fig 3F**). Taken together, these results show a decorrelation between visual input and behavioral state or context, which weakens the hypothesis that neural signatures of behaviors or contexts in TEO and vlPFC are entirely explained by unique visual inputs or movement patterns.

Although movements and field of view do not explain all neural variance in these brain areas, it remains unknown how much of the variance is indeed explained by visuomotor contingencies during natural behavior in primates. Using a multi-linear ridge regression method[32,51], we quantified the relative neural variance explained by behavioral states, movement patterns (17 key points across the whole body, **Fig 6A**), and visual field (see **Methods**). Replicating previous findings in macaques PFC during laboratory tasks [32], we found that natural movements explained a large part of the neural variance in both vlPFC and TEO (Full contribution; light green, unique contribution; dark green; **Fig 6E**). However, after accounting for whole body movements and field of view, behavioral states still uniquely explained part of the neural variance (dark green; **Fig 6E** bottom). To further quantify the contribution of movements and field of view to neural coding, we regressed out those two sets of variables from neural population activity and re-ran the decoding analysis of behavior depicted in **Figure 3E**. We found that regressing out those variables decreased decoding accuracy by 7.5% on average, whereas regressing out variation related to ethologically-defined behavioral states decreased accuracy by 35.6% (**Fig 6F**). In sum, patterns of neural activity related to behavioral states in distinct social contexts could not be fully explained by the sensorimotor parameters we measured and therefore at least partially represent species-typical behavioral states and social contexts independent of immediate sensorimotor contingencies. We also note the presence of strong movement signals in those freely-moving animals, even in a visually-defined area like TEO, which has important implications for current laboratory and future freely-moving experiments

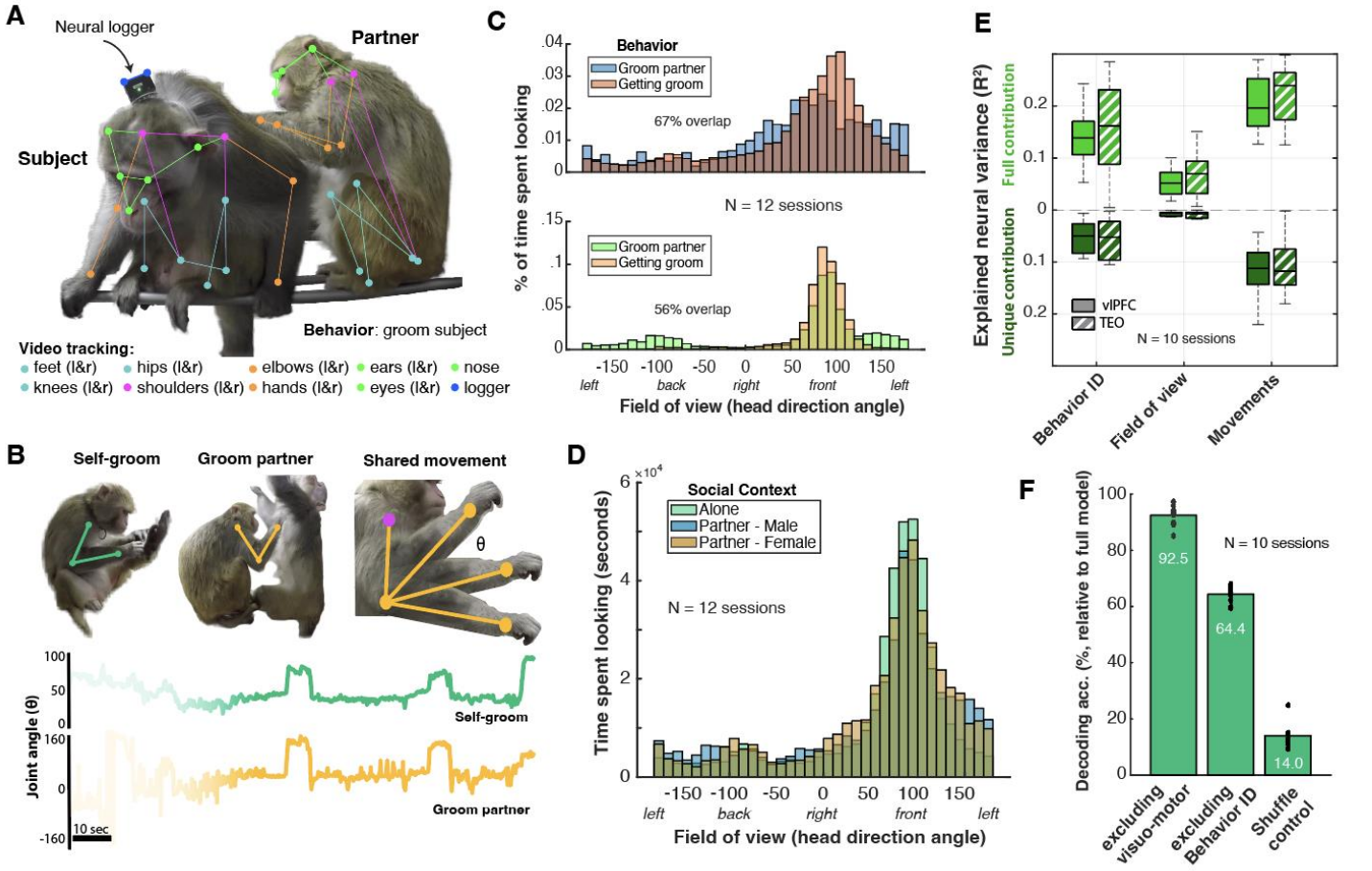

Fig 6. Patterns of population neural activity are not reducible to visual field of view or movement kinematics. (**A**) Schematic of movement quantification including 17 body landmarks, head position, and head direction (extracted from neural logger position). (**B**) A comparison of elbow joint angle during two behaviors, self-groom and groom partner. Top: depiction of the stereotypic self-groom behavior (left), groom partner (middle), and the shared motion pattern of shoulder-elbow-wrist across both behaviors (right). Bottom: plot of joint angle θ over time for self-grooming (green) and groom partner (yellow). Shaded portion indicates onset and offset of both behaviors. (**C**) Field of view varied substantially within a given behavioral state and overlapped across behavioral states, decorrelating the two. Histograms of field of view during getting groomed vs. rest (top) and groom partner vs. self-groom (bottom). (**D**) Field of view largely overlapped across all three social contexts, decorrelating social context coding from visual inputs. (**E**) Neural variance explained by behavioral states (Behavior ID), field of view, and movements obtained by regressing population activity onto those variables over the time-course of an entire session. Behavioral states explained a large part of the neural variance (Full contribution; top), even after removing variance explained by movements and field of view (Unique contribution; bottom) (quantified with ridge regression as in Musall et al. 2019[51], see Methods). (**F**) Decoding accuracy of an SVM decoder predicting the behavioral ethogram (as in **Fig 3E**) from neural population activity, while controlling for visual and motor confounds. Scores relative to the full model shown in **Fig. 3E**. Note that we could not perform video tracking on 2/12 sessions due to missing videos from appropriate angles (see **Methods**). Thus, panels E-F contain data from 10 sessions.

Discussion

The neural mechanisms underlying natural social behaviors in humans and non-human primates have been notoriously difficult to study in ecologically-valid environments. Here we used an ethological approach, new wireless neural data-logging technology, and computer vision techniques to investigate how cortical activity relates to natural behavior in freely-moving, socially-interacting macaques. We manipulated social contexts and exposed monkeys to social threats to investigate the neural basis of affiliative and aggressive behaviors. We found that activity of single neurons in both prefrontal and inferotemporal cortices were broadly modulated by a wide array of behaviors, with affiliative behaviors characterized by global suppression and aversive behaviors by global

excitation. Furthermore, individual neurons were modulated by a large number of behaviors compared to laboratory task variables, suggesting broadly distributed rather than sparse neural coding of natural behaviors in the cortex. The presence and identity of surrounding monkeys strongly structured neural population coding of behaviors, and both behavior and social contexts were highly decodable. Monkeys spontaneously engaged in remarkably reciprocal grooming interactions, which were unlikely to occur without a form of mental accounting. Neural populations tracked net number of grooming bouts given and received as well as elapsed time, a potential mechanism supporting this reciprocity. Threats from a human intruder provoked behavioral agitation and strong neural responses in subjects, which were buffered by the presence of a partner. Neural responses were similar when the subject monkey or his partner were threatened, a neurophysiological 'mirroring' consistent with empathy. Importantly, neural signatures of behaviors and social contexts were irreducible to measured visuo-motor contingencies, supporting the experimental feasibility of investigating brain activity in freely-moving primates.

Contrary to expectations, populations of neurons in TEO and vlPFC carried comparable information about behavioral states, social contexts and records of past interactions. Given the anatomical and functional distinctions between these areas, it seems likely that the modulations we observed occur in many other cortical areas as well. Our findings extend prior work in rodents showing brain-wide behavioral state modulations as a function of movement or arousal in primary sensory areas[51,52,54,55]. The multiplexing of neural representations of behavior and social context in a visual processing area such as TEO may be a mechanism through which the brain contextualizes sensory inputs to facilitate generation of adaptive behavior. Neuronal activity patterns in TEO and vlPFC may be distinct at shorter timescales or in contexts we did not examine here. The origins and implications of apparently redundant neural signals across brain areas needs further investigation[56,57].

The neuroethological approach we adopted here is based on the premise that a species' neural circuitry is refined by evolution to support specific functions with adaptive significance in the natural world[1,58,59]. This approach revealed neural signatures of specialized behaviors in multiple species, including barn owls, songbirds, electric fish and bats[58,60,61], which might have otherwise remained undiscovered through traditional approaches using highly-controlled behavioral tasks[1,62]. In this study we found widespread, highly-structured neural signatures of natural behaviors and social contexts that permeate the day-to-day lives of primates. The highly-distributed coding we observed contrasts with ubiquitous observations of sparse coding[33], and this discrepancy may reflect the limited and constrained nature of laboratory tasks as the source of neurophysiological data upon which sparse coding models are based. Foundational theories of brain functions may need revision as neurobiological investigations are extended to the complexity of natural behavior. Finally, enabling macaques to express their natural behavioral repertoire allowed the study of fundamental, fitness-enhancing mechanisms supporting social relationships in primates at the single neuron level. This work lays the foundations for an ethological turn in primate neuroscience[62] to unravel the neurobiological mechanisms that support our own rich and complex social lives.

Acknowledgments: We thank Robert Seyfarth, Adam Lowet, Richard Lange, Juan I. Sanguinetti-Scheck, Carlos Ponce & Merhdad Jazeyari Labs for conceptual, theoretical and methodological advice, Xiaowei Jiang for help with pose-tracking, and Jordan Matelsky for artwork for the human-intruder paradigm.

Funding: R01MH095894, R01MH108627, R37MH109728, R21AG073958, R01MH118203,866 R56MH122819 and R01NS123054 to M.L.P., Blavatnik Family Foundation Fellowship to CT, Canada Banting Fellowship and Human Frontier Science Program Fellowship to S.T.

Author contributions: Study conceptualization: CT, ST, MLP; Surgical implantation: ST, KG; Data collection: CT, FP; Behavioral labeling: CT, AA, ST; Video motion tracking: FP; Data analyses: CT, ST, RWD, FP; Figure editing: CT, ST; Funding acquisition: CT, FP, ST, MLP; Writing of manuscript: all authors reviewed and approved this manuscript.

Competing interests: MLP is a scientific advisory board member, consultant, and/or co-founder of Blue Horizons International, NeuroFlow, Amplio, Cogwear Technologies, Burgeon Labs, and Glassview, and receives research funding from AIIR Consulting, the SEB Group, Mars Inc, Slalom Inc, the Lefkort Family Research Foundation, Sisu Capital, and Benjamin Franklin Technology Partners. All other authors declare no competing interests.

Data and materials availability: Data will be available on Open Science Framework platform and code on GitHub at https://github.com/camilletestard/Datalogger upon official publication.

SUPPLEMENTARY MATERIAL

Materials and methods

1. Subjects:

Four adult rhesus macaques (*Macaca mulatta*) participated in the experiment, two males, from which we recorded neural activity, and their two female enclosure-mates, which served as partners. No neural data was recorded from the females. Due to past aggressive interactions between members of each pair, males and females in this experiment were only allowed to be physically in the same space under the supervision of the experimenter, and all interactions were recorded.

Animals were trained using positive reinforcement via clicker training to enter a primate chair (Hybex Innovations, Canada) where we then lowered a custom-built plexi-glass face shield to stabilize the head for up to 5 minutes while positioning the neural data-logger device (see details below) and/or for implant maintenance. No other head-restraining methods were used for this experiment. After the data-logger was installed, males were reintroduced into their home enclosure in the colony room to begin the experiment. Subject monkeys underwent no further training, and no food or liquid controls were used for this experiment. The entire study lasted 6 months (mid-March to mid-September 2021).

2. Surgical procedures:

Surgeries were performed by senior research investigator S.T. and veterinarian K.G. Surgical plans were prepared with the help of brain MR images obtained on a Siemens PRISMA 3T scanner. T1-weighted images (MP-RAGE) with and without gadolinium enhancement (Gadovist®, Bayer, Germany) were obtained to reconstruct the 3D cortical surface and vasculature (Brainsight Vet 2.4, Rogue Research, Canada; see Fig 2A). Custom Utah arrays

(Blackrock Microsystems, UT) were designed on the basis of local morphology in the region of interest for each monkey. The aim was to cover optimally the regions of interest (ROIs: areas 45 and TEO) while avoiding major blood vessels. For this reason, we targeted the right hemisphere for monkey A and the left hemisphere for monkey H. All surgeries were carried out under isoflurane anesthesia and under strict sterile conditions with the assistance of experienced veterinary staff. The neural recording implants (Utah arrays) and surgical procedure are consistent with surgeries that are FDA-approved for use in human patients. The animal's head was positioned in an adjustable holding frame (Jerry-Rig, NJ) and a midline skin incision was made to expose the dorsal aspect of the skull. The temporalis muscles were retracted and a square-shaped craniotomy was made over the ROIs, based on MRI coordinates, with a dental drill equipped with a diamond round-cutting burr (Horico, Germany). The dura-mater was exposed and a dural flap was performed extending ventrally. Direct visualization of cortical landmarks, including the arcuate sulcus and the sulcus principalis for area 45, and superior temporal sulcus and inferior occipital sulcus for area TEO, was used to determine implantation sites. The arrays were carefully positioned over the two ROIs and implanted using a pneumatic inserter held by a flexible surgical arm. The dural flap was closed with 5-0 Vicryl® sutures. The bone flap was thinned with a drill and replaced over the craniotomy and secured to the skull with low-profile titanium plates and screws (DePuy Synthes, IN). A Cereport connector was secured dorso-caudal to the skull opening using eight 1.5mm diameter titanium screws with a length determined by the skull thickness as measured by pre-operative MRI. The two reference wires were inserted between the dura and the cortex and the exposed portion of those wires and of the array wire bundle were coated with a thin layer of Geristore (Denmat, CA). The muscle, fascia and skin were closed in anatomical layers with absorbable 3-0 Vicryl® sutures and the Cereport connector protruded through a small opening in the skin. For antibiotics, patient received cefazolin (225 mg/mL) at 20 mg/kg IV intraoperatively q 2 hrs, and 20 mg/kg ceftiofur CFA (Excede(R), 100 mg/mL) SC once post-operatively. The anti-emetic maropitant (Cerenia(R), 10 mg/mL) was administered at a dose of 1 mg/kg SC pre-operatively. Analgesia consisted of buprenex 0.02 mg/kg IM once pre-op, then BuprenorphineER (ZooPharm(R), 10 mg/mL) 0.15 mg/kg SC once at extubation. Anti-inflammatories/analgesics: meloxicam 0.2 mg/kg at surgery and 0.1 mg/kg SID x 4 days. Dexamethasone SP 0.5 mg/kg BID on day of surgery. The monkeys recovered for two weeks before the first recording session. No headposts were implanted for this study and no acrylic or dental cement was used (see **Fig S1** for surgical outcomes).

3. Neuro-behavioral recordings in the home enclosure

a. Setup and behavioral manipulations

We recorded neural activity from freely-moving, spontaneously behaving rhesus macaques in their home enclosure. This protocol minimized disruption of the monkeys' daily routines, reducing stress as well as training time, thereby promoting expression of the natural behavioral repertoire. The two pairs were located in neighboring enclosures (i.e., side-by-side). We used fully-occluding black room dividers (Versare MP 10 Economical Portable Accordion Partition) to visually isolate our subject monkeys from the other monkeys in the colony room, which contained a total of 15 male and female rhesus macaques. Subject monkeys could hear but not see the other monkeys in the room. Vocalizations and other sounds emitted by non-experimental macaques were captured through microphones but not analyzed for this study.

Each session began with a 15 min installation phase in which we: 1) Installed 8 battery-powered GoPro cameras (HERO7) around the subject's home enclosure and the neighboring one at locations optimized to monitor all

subject monkeys' behavior (see **Fig 1A** for camera positions); and 2) transferred the subject monkey from his enclosure into a primate chair to install and secure the data-logger. Once the data-logger was secured to the head, the subject monkey was returned to his enclosure and simultaneous neural and video recordings began. Both steps were done in parallel by two experimenters to reduce preparation time. The two human experimenters were seated in front of the experimental enclosures and remained visible to the subject monkeys during the entire length of the session.

Each recording session lasted 2.5 hours and was divided into three experimental blocks, in which we varied social context. There were two 45 min "paired blocks," in which the male subject was paired with his female partner, and a 1 hour "alone block," in which the subject was fully visually isolated from all other monkeys. During paired blocks, subjects and their female partners had access to the full enclosure space (height: 2.5 m, width: 2 m, depth: 1 m) and were free to interact. Subject monkeys also had visual access to the adjacent enclosure where only one monkey, dubbed the "neighbor", was visible at any given time. Subject and neighbor monkeys could not touch each other but could observe each other through the caging. The neighbor monkey was either the male or the female from a different male-female pair. Neighbor identity was switched for each of the two "paired blocks" (e.g., if the neighbor was male in the first "paired block", the neighbor was female in the second). During "alone blocks", the subject only had access to half of the enclosure space (height: 2.5 m, width: 1 m, depth: 1 m) and no visual access to other monkeys. **Figure 1A** provides a schematic of the experimental set up and block design. Block order was varied pseudo-randomly across sessions (see **Appendix 4** *"Intervention schedule"* for more details).

Within each block, we performed two additional manipulations. First, we provided naturalistic foraging material at the beginning of each experimental block. We used artificial turf foraging trays (© Otto Environmental) in which we hid a variety of small food items (on average 300 small items, <50g of rewards per session). Food items included pieces of dried raisins and other berries, small spherical fruit pellets (Bio-serv 190mg fruit pellets), pieces of marshmallow, peanuts, and yogurt drops. By hiding numerous small food items (max 5mm in diameter) inside these foraging trays, we ensured that full depletion of the tray required at least 10 min of continuous foraging. Subject monkeys foraged in multiple bouts throughout sessions (**Fig 1B**). Successful foraging required precise motor coordination to grasp the small hidden items, akin to precision grasps used for grooming.

Second, we performed human intrusions to elicit aggressive and/or defensive behaviors from our subjects, who otherwise would very rarely exhibit aggressive behaviors towards other experimental monkeys (see **Fig 4B)**. Human intrusions were 30 second-long interventions in which the same male experimenter approached the front of the experimental enclosure and continuously displayed open mouth threats and confrontational stares towards either the subject (threat to subject) or his female partner (threat to partner). Open mouth threats are common aggressive displays among rhesus macaques, and human threats elicited strong responses from the subject monkeys (irrespective of whether the target was the subject himself or his partner, **Fig 4B**). Within any given session we performed 6 human threat interventions, 3 towards the partner and 3 towards the subject, across the three experimental blocks. Threats were either performed while the subject and partner monkeys were paired or when the subject was alone to assess the effect of social context. For more details refer to the intervention schedule in **Appendix 4**.

At the end of each recording session, there was a 15 min breakdown phase in which we transferred the subject monkey into the primate chair, stabilized his head using the plexi-glass face shield to remove the data-logger, and performed routine cleaning of the implant by applying alcohol over and around the connector, flushing with distilled water and then with chlorhexidine. Once the connector was fully dried, we placed a protective cap over it and transferred the animal back into his home enclosure. We removed all cameras and occluding panels to return the colony room to its baseline state at the end of each session. We then proceeded to upload the video and neural data collected to a centralized server (Dropbox©).

b. Neural recordings and spike detection

We used chronically-implanted Utah arrays for neural data recording of single neuron spiking activity. Each monkey was implanted with two 64-electrode arrays, one in frontal cortical area 45 and one in temporal cortical area TEO. Monkey A was implanted in the right hemisphere and monkey H in the left hemisphere to avoid major vasculature on the ROI (**Fig 1A**). The two arrays were coupled to a single Cereport connector with 128 channels. We used a novel custom adapter to connect the Cereport to a neural data-logger to enable range-free, wireless chronic recordings (Spikelog128, Deuteron Tech., Israel). The raw signal was bandpass-filtered (500 Hz to 7000 Hz) and digitized (16 bits) at 32,000 samples per second on the head mounted data-logger. Digitized data was saved on a microSD card (Kingston, 512Gb) inside the data-logger. This allowed for a light (33 g), miniaturized (31x32x27mm), fully wireless neural recording system, enabling the animal to express unconstrained natural behaviors (**Fig S1**). We used a tablet (Surface Pro 7, Microsoft Inc.) to wirelessly communicate with the data-logger using the Deuteron software via a radio-transceiver box (ST4). During each session, we sent event-markers for behavioral and camera recording events through radio transmission. Event-markers were synchronized to the master clock of the neural recording system.

For each recording channel, action potentials ("spikes") were detected offline based on a channel-specific voltage threshold 3.7 times the root mean square of the noise amplitude (Offline Sorter version 4, Plexon Inc. TX). Waveforms were manually spike sorted using Offline Sorter. Well-isolated single units as well as multi-unit clusters were manually classified on each channel and saved for future analyses in MATLAB (MathWorks, MA). Assuming we recorded entirely different neurons on each session, we recorded n = 3,689 units (including single and multi-units) over 12 sessions (6 per monkey, mean of 307.42 units per session, SD=19.67) during 1 month of recording. Neuron count remained stable throughout the duration of recordings (**Fig S1**). Two additional sessions were recorded but the neural data was invalidated due to liquid insertion in the datalogger causing large amounts of noise in the signal. These sessions were kept for behavioral analyses.

c. Behavioral monitoring

Prior to the start of the experiment, we conducted 10 hours of preliminary observation of the subject monkeys (5 x 2-hour sessions, 3 sessions for monkey A, 2 sessions for monkey H) to establish a behavioral ethogram. Our group has conducted extensive field behavioral research on a free-ranging colony of rhesus macaques living on the Cayo Santiago island, Puerto Rico, for over a decade (ethogram for Cayo macaques in **Appendix 1**), and we leveraged this experience to devise an ethogram for our study. Our final ethogram included 24 behaviors that recapitulate behaviors observed by our team in the free ranging population, including behaviors such as "foraging", "groom partner", "getting groomed", "lip-smacking", "submission" and "mating" (see **Appendix 3** *'Ethogram'* for a complete list of behaviors and accompanying detailed descriptions). The Deuteron custom software allowed us to send event-markers through radio-transmission during recordings. During the experiment, a human observer (the same across all sessions) time-stamped behaviors of the subject monkey, marking the start

and end of behaviors from the ethogram, as ethologists routinely do when observing primates in the wild using continuous focal animal sampling[63].

To complement human-based live observations of natural behaviors, we also video-recorded the behavior of the subject monkey, its partner, and neighbor using 8 GoPro HERO7 cameras (1080p resolution, 29.97 frames per second). Cameras were synchronized to each other and to the master clock of the neural recording system using a GoPro Smart remote via bluetooth with sub-second temporal resolution (<0.5 sec, benchmark established through extensive testing by the authors prior to the start of the experiment). To ensure accurate synchronization, we performed two additional synchronization checks during each session, using an auditory signal captured by the cameras and the Deuteron event log. Cameras were positioned to ensure maximum coverage of the subject's home enclosure, his partner and the neighbor.

To ensure second-resolution accuracy, behavioral events timestamped live during the session were adjusted post-hoc through manual video scoring by two expert human observers (CT and AA) with extensive primate field observation training. Inter-observer reliability over 3 jointly-scored sessions was 96%. The remaining 11 sessions were coded by only one of the two expert observers (AA) who was blind to all subsequent neural data analyses. We labeled the behavior of the subject, partner, and neighbor to the second resolution. Only the behavior of the subject was related to neural activity for this study; the behavior of the partner monkey will be the focus of future work.

4. Description of behavior

a. 'Rest' as a baseline state

We categorized timepoints when monkeys did not engage in overt behavior (as defined by our ethogram) as 'rest'. Rest typically manifested as a monkey sitting and looking around, and thus should not be confused with sleeping. Our subjects were fully awake and behaving for the entire length of the experimental sessions. In subsequent analyses we used rest as a "baseline" measurement of neural activity, unless specified otherwise.

b. Comparison with ethogram used with Cayo Santiago free-ranging macaques

Our laboratory setup allowed our subject monkeys to express a breadth of natural behaviors which largely overlaps (84%) with the breadth of behaviors observed in a free-ranging colony of rhesus macaques (**Appendix 1**, [64]). To quantify this overlap, we made a list of all behaviors in the Cayo Santiago ethogram and counted the number of behaviors which were also exhibited in the laboratory (see **Appendix 2**).

Cayo-Lab Overlap = [# behaviors exhibited in the lab / All behaviors exhibited on Cayo]

c. Co-occurrence of behaviors

The subject occasionally engaged in multiple behaviors simultaneously (e.g., "scratch" and "getting groomed"). In these cases, we utilized the following criteria for choosing the behavior to code: When a behavior co-occurred with "proximity", "rowdy room" (loud noise in the colony room), or "other monkeys vocalize", we prioritized the former behavior (most common case). In all other cases of co-occurrence of behaviors (< 2% of the time), we established a "hierarchy" of behaviors that take precedence (e.g., getting groomed takes precedence over scratch). See **Appendix 3** *'Precedence'* for more details. The same hierarchy of behavior was applied to the partner's behavior.

d. Exclusion of behaviors in analyses

During behavioral labeling, "proximity", defined as being within arm's length of another monkey, was coded as part of the ethogram. In subsequent analyses, we pooled "rest" and "rest in proximity" because we judged the recording arena not large enough to make a meaningful distinction between them (paired monkeys were essentially always in proximity). The majority of our analyses used "rest" epochs as baseline and excluded behaviors performed by other monkeys in the colony (e.g., "Other monkeys vocalize" and "Rowdy Room", see **Appendix 3** for definitions), and rare behaviors (which happened for a duration of <30 s in a given session, or < 10 times across all sessions, see **Appendix 3** *'Behavior lists'* for a list), unless specified otherwise. These exclusion criteria resulted in the majority of our analyses considering 17 of the 24 total behaviors observed across sessions (see **Appendix 3** *'Focus of analyses'*). Typically, 12 out of these 17 behaviors occurred frequently enough to be analyzed in any given session.

e. Behavioral frequency and transition matrix

We combined behavioral data from all sessions and computed the proportion of time spent in each behavioral state: proportion for behavior A = [# of seconds in behavioral state A / total # of seconds] (**Fig 1C**). We then computed behavioral transition matrices for each monkey in which each cell is the total count of transitions from the row behavior (y-axis) to the column behavior (x-axis) across all sessions (**Fig S1**). Transitions excluded "rest" epochs, behaviors performed by other monkeys in the colony ("Other monkeys vocalize" and "Rowdy Room"), as well as short event behaviors (1-3 s in length: "vocalization", "lip smack", "anogenital investigation" and "scratch"). Transition plots are pooled across monkeys and thresholded by frequency per behavior in **Fig 1D** (>20% transitions), and un-thresholded in **Fig S1**.

f. Grooming categories

It is possible that neural responses to a behavior could be modulated by preceding events. In our experimental sessions, we were able to identify three grooming contexts that are known to be important from decades of field observations of primates in the wild [65]: 1) Whether grooming was initiated by the partner or the subject; 2) Whether a grooming bout immediately followed a previous one, i.e. reciprocal grooming and 3) Whether grooming occurred after aggression (see **Appendix 3** *'Grooming categories'* for detailed description). Note that these categories are not mutually exclusive. For example, a grooming bout can occur after aggression and also be initiated by the subject.

g. Grooming reciprocity

Grooming reciprocity was calculated using two metrics: reciprocity (1) and directional reciprocity (2).

(1) Reciprocity = 1 - abs(Groom given - groom received)/Total grooming. Values will range between 0 –fully one-sided– and 1–perfectly equal.
(2) Directional reciprocity = 1 - (Groom given - groom received)/Total grooming. Value will range between 0 and 2, where 1 = perfectly equal, <1 more was given than received and >1 more was received than given.

Note that grooming duration given vs. received or number of grooming bouts in each direction could be used to compute reciprocity. We refer to the former as "groom duration reciprocity" and the latter as "bout number reciprocity".

To investigate reciprocity in grooming bout number and duration between members of a pair, we considered unidirectional grooming bouts separated by less than 10 seconds to be part of the same bout. Alternating bouts consisted of grooming bouts preceded by grooming in the opposite direction (Give - Receive - Give). When examining the distribution of inter-bout intervals (IBI), we identified a bi-modal distribution with very short IBI and much longer ones (**Fig S4A**). We defined alternating bouts separated by <20 sec as "turn-taking".

To characterize how reciprocity developed and fluctuated over the course of a session, we computed a running reciprocity metric that considers all grooming seconds up to the current time in the session (**Fig 4E**). In all sessions grooming occurred for at least 2500 sec (some sessions extended grooming for longer). Therefore, to compute

average running reciprocity across sessions, reciprocity was computed for the first 2500 sec of grooming within a session and aligned to "Start of grooming".

5. Simulations for grooming reciprocity

Simulations were used to establish the distribution of reciprocity and turn-taking assuming monkeys groomed at random (null distribution). If the observed reciprocity and turn-taking fell outside this distribution ($P < 0.05$), we concluded it was unlikely monkeys groomed randomly and instead surmised grooming decisions were made to reciprocate and/or take turns. All simulations were run 10,000 times to obtain p-values.

a. Reciprocity in bout number given random allocation of grooming

To generate a null distribution for bout number, we chose to model grooming as the combination of an initiation process and a duration process. At each moment a monkey can choose to initiate grooming his partner or not. We modeled this choice by using a random draw from a uniform distribution to set the probability of choosing to start grooming and then taking a random draw from a Bernoulli distribution with that probability (i.e. "flipping a coin" with probability *p* of initiating grooming). If the monkey did not initiate grooming, we conducted the same process to see if his partner would initiate grooming. If neither monkey initiated grooming, we moved on to the next moment and repeated the simulation. If either monkey initiated grooming, we took a random draw from an exponential distribution with a expected duration of 100 seconds and set the duration of the initiated bout to this random draw. We continued the simulation until 45,000 seconds (approximately the length of all sessions combined for one monkey) had elapsed from time waiting for either monkey to initiate grooming and total duration of the grooming bouts. We then tallied the number of grooming bouts for each monkey and calculated the reported statistics in **Fig 4C** top panel. Note that the range of total number of grooming bouts from this simulation matched the observed total number (range: 153-231 bouts).

b. *Probability of turn-taking given random ordering of bouts given and received*

To obtain a null distribution of turn-taking, we shuffled the directionality of observed grooming bouts (i.e. give vs receive). Bouts that alternated in direction and were separated by less than 20 sec were labeled as "turn-taking" in the shuffled data. We then calculated the proportion of turn-taking bouts out of all grooming bouts and compared this null distribution to the observed proportion of turn-taking (**Fig 4C** middle). Finally, we calculated the probability of observing the true proportion of turn-taking in this null distribution (p-value).

c. Reciprocity in groom duration given random allocation of grooming length to observed grooming bouts

We generated a null distribution of reciprocity in groom duration assuming monkeys did not track time. We maintained the empirical frequency, timing and directionality of bouts but randomly sampled durations from the observed distribution of grooming bout durations (**Fig S4**). This way we kept the natural statistics of the grooming behavior of our subjects. We then compared this null distribution to the observed reciprocity values, both within and across sessions, and calculated the probability of observing the observed reciprocity..

6. Behavioral quantification:

a. Monkey detection and pose estimation

To detect monkey position and estimate their pose, we trained a monkey detection model and a pose estimation model using the *mmdetection* and the *mmpose* Python libraries (Python version 3.8) [66,67] respectively. Combining these models ultimately enabled us to quantify the position of 17 body landmarks in freely-interacting monkeys (see **Appendix 3** *'Visuo-motor measures'* for full list) by following the training procedure we will now outline. For both models, we leveraged standard data augmentation techniques as well as transfer learning [68]. We first trained each model on the MacaquePose dataset [69], and then supplemented training with annotated images from our dataset. We trained the monkey detection Faster R-CNN model [70], and then the pose estimation model HRNet-W48 [71], which has been shown to perform well in tracking myriad primate species [72]. Pretrained models for both

the Faster R-CNN and the HRNet-W48 are publicly available for training in the *mmdetection* and *mmpose* Python libraries respectively. For the monkey detection model, we labeled and split 3,082 images (3,962 monkey instances) of freely-interacting monkeys into training (70%), validation (15%), and testing (15%) sets using Roboflow [73]. For the pose estimation model, we labeled and split 4,889 images (6,084 monkey instances) into training, testing, and validation sets using the Scikit-learn Python package [74]. We used mean average precision (mAP), precision, and recall metrics to evaluate the monkey detection model, and mean average precision to evaluate the pose estimation model. The trained detection model returned a mAP of 99.4%, precision of 98.5%, and recall of 99.3%, and the trained pose model returned an mAP of 93.2% across body landmarks. After training these two models, we analyzed the video data using a three-stage pipeline: 1) detect monkeys, 2) assign their bounding boxes IDs and 3) quantify their poses. Detection of the monkeys was handled directly by the monkey detection model. The subject monkey (ID 1) and partner monkey (ID 2) bounding boxes were assigned based on camera angles during the "alone" block, which we verified manually. If the camera angle faced the subject monkey during the alone block, we assigned all bounding boxes during this block ID 1, and if it faced the partner monkey, we assigned all bounding boxes during this block ID 2. During social blocks, we employed a set of heuristics that relied on the presence of a data-logger to assign IDs to the bounding boxes of detected monkeys. Namely, we assigned IDs to monkey bounding boxes based on the top center point of each bounding box and its proximity to the data-logger bounding box top center. For frames in which both monkey bounding boxes and data-logger bounding boxes were detected, we computed the top center point of each bounding box and assigned the monkey bounding box "1" to the monkey bounding box top center that was closest to the data-logger bounding box top center. For frames in which the data-logger was not detected, we used previous bounding box data to assign IDs based on closest distance to bounding boxes in previous frames. Once the IDs were assigned, we performed pose estimation on the monkeys within each bounding box. To smooth the pose tracking results, we applied a Savitzky-Golay filter consistent with prior primate pose estimation studies [75]. Of the 7 cameras surrounding the monkey enclosure, we analyzed behavior from the side angles (four out of seven camera angles), which had the better overall view of the animals' pose. For each predicted keypoint, the pose estimation model returned a corresponding confidence score as a measure of how likely it is that the keypoint exists in that position. The confidence score is based on the output of a "softmax" activation function that assigns a probability from 0 to 1 to each possible keypoint location in the image; the higher the probability, the higher the confidence score. After inspection, we considered a confidence cutoff value of 0.2 to be appropriate (see sample tracking results in **Movie S5-8**) and conditioned the X,Y coordinates using this threshold for future analysis (i.e. all tracking data with a lower confidence score than our cutoff value were discarded from downstream analyses).

b. Field of view quantification

To quantify the field of view of each subject monkey, we used the pose tracking software DeepLabCut to track the top and bottom positions of the data-logger (DeepLabCut version 2.2.2; [76,77]). We labeled 6,486 images (2,423 monkey instances) taken from top-down view videos across all 12 sessions and used 95% of these images for training. We trained a ResNet-50 neural network to perform pose estimation with default parameters for 2 million iterations, achieving a mean average Euclidean error (MAE) training error of 2.66 pixels and MAE test error of 5.54 pixels. Like the previous pose tracking model, this neural network outputs a likelihood score for each predicted keypoint. As a confidence metric, we used a p-cutoff, a parameter that determines the confidence threshold of each keypoint, of 0.7 to condition the X,Y coordinates for subsequent analyses. After training, we used this model to track data-logger position from the held out sessions. Using the front and back corner coordinates of the data-logger, we calculated the angle, in degrees, between these two points using the *atan2d* function in Matlab. The back corner of the data-logger was used as a reference point around which the front corner rotates. This rotation angle is equal to the orientation of the head in space, which we termed "field of view". Sample tracked results are shown in **Movie S9**.

c. Metrics and missing data for movement and field of view tracking

For each session with appropriate side and top-down view videos (used for full body and logger tracking, respectively), we extracted various visual and motor metrics, including animal's x,y position, full body key points,

head movement, velocity, acceleration, and head direction (see **Appendix 3** *'Visuo-motor measures'* for a full description). We had to exclude 2/12 sessions for analyses including full body tracking due to missing side view videos on these sessions.

Our subject monkeys sometimes were out-of-sight of camera coverage leading to some key points becoming invisible for periods of time. When these moments occurred, our tracking models attempted to infer the position of invisible body-parts based on a full skeleton model of the animal. It was not always possible for our models to make a high certainty inference; therefore there is data missing from our movement tracking. Using a 0.2 confidence score for pose tracking with *mmdetection* and *mmpose* and 0.7 score for data-logger tracking with DeepLabCut, we had 78.98% missing data on average across sessions (SD 28.34%). We omitted these time-points from subsequent analyses.

d. Manual scoring of agitation during human threat paradigms

We manually scored the behavioral response to human threats from video recordings by considering the occurrence of three types of social behaviors by the subject monkey: 1) attacks: defined as rapid arm gestures by the monkey aimed towards the human intruder, 2) dodges: defined as rapid head and body movements to achieve an aggressive posture 3) submissions: defined as a presenting hindquarters to the human intruder. The summed frequency of these three behaviors during a single 30 sec human intruder bout was considered the "agitation score" for this bout, such that a high score corresponds to a high agitation level and a low score low agitation. Each bout was classified as either belonging to the "alone" or "paired" category, depending on whether the monkey was alone or paired during the bout. The same scoring procedure was repeated during threats directed toward the partner monkey (**Fig 5B**).

7. <u>Preprocessing steps for subsequent analyses of neural activity:</u>

For each session, we aggregated the spike counts of each neuron into time bins of 1 seconds except for analyses involving movements where we binned at the camera frame-rate or 29.97 Hz. This process produced N sets of 1 x T spike count vectors where N is the number of neurons and T is the total number of time bins given the temporal resolution. We then convolved these spike count vectors with a 1 time bin standard deviation gaussian kernel to obtain the smoothed approximate instantaneous firing rate of each neuron. All downstream analyses used instantaneous firing rates as input unless specified otherwise. Units that had very low (<0.1Hz) or very high mean firing rate (>150Hz) were excluded from our analyses.

We also created a 1 X T current behavior vector by assigning each time bin a numeric label which corresponded to a particular behavior from our ethogram (**Appendix 3**). Accordingly, these preprocessing steps created a "neural firing matrix" of size [#units X Time (at desired temporal resolution)] and a "label vector" of size [1 X Time (at the same desired temporal resolution)]. All subsequent analyses were performed on this neural firing matrix and label vector. All analyses were performed using Matlab 2021b unless indicated otherwise.

8. <u>Single unit responses across macaques' natural behavioral repertoire:</u>

To explore the response profiles of single units across macaques' natural behavioral repertoire we first extracted the empirical distribution of firing rates of all units during each individual behavior. Each sample in these distributions consists of the firing rate recorded for 1 sec during the session; e.g., if grooming occurred for 1000 seconds during a session, the distribution of firing rate during grooming will contain 1000 data points. We then performed the same operation during "rest" epochs, our baseline, and compared this baseline distribution to the distributions we observed for each behavior **(Fig 2C**). Specifically, we used Cohen's d to quantify the standardized mean difference in firing rate during each behavior compared to rest (**Fig 2D**) via the following formula:

$$d = (M_1 - M_2) / s_{pooled}$$

We then used two-sample t-tests (N *t*-tests= number of neurons x number of behaviors) to determine whether the differences in mean firing rate as calculated by Cohen's d were statistically significant (**Fig S2C**). To control for false positives, we used Benjamini & Hochberg's (1995) false detection rate (FDR) procedure [78] as implemented in the Matlab function *fdr_bh* [79] and used FDR-corrected *P*-value of 0.01 as a significance threshold. We considered a unit's activity to be significantly modulated by a behavior if FDR-corrected *P*-value<0.01 (**Fig 2F**). Sample size influences *P*-values, so we repeated our analysis to find the number of behaviors a given neuron is responsive to by subsampling our data to have 100 observations (seconds) per behavior (**Fig S2B**). We also repeated these analyses for well-isolated units only and found qualitatively similar results (**Fig S2C**). To quantify global trends across all neurons we also computed the mean z-scored firing rate of individual units for each behavior and plotted the resulting distribution across all units in **Fig 2E**.

9. Linear decoding of behavior and context based on neural population activity

To assess what information a hypothetical downstream brain region could linearly readout from the recorded neural activity, we ran a series of decoding analyses. In each analysis, we used a linear support vector machine (libSVM [41]) with 5-fold cross-validation. Note that 5-folds were created by splitting the session length into 5 chunks rather than random sampling of indices (which is the default in Matlab but can lead to overfitting). We trained the SVM on simultaneously recorded units, i.e., "the neural population", to get an estimate of overall linearly decodable information contained in the entire population of recorded units (rather than assessing individual units separately). We used a shuffled, hold-out cross-validation procedure where, for each fold, time points from the session were randomly sampled and assigned to either the training or testing set (training to test split was 80% to 20%). The accuracy of the trained model was calculated based on the number of correct predictions on the testing set (correct predictions / all predictions). There were large discrepancies in the number of observations for each variable we were attempting to decode. To account for how this difference could bias performance, we balanced the number of observations per variable (e.g. current behavior or social context) by randomly subsampling the variables with more observations so that each had the same number of observations as the least observed variable. To account for variance in performance caused by random subsampling, we ran 100 iterations of each SVM and computed the mean decoding accuracy across all iterations. We calculated empirical chance performance of the decoder by randomly permuting the variable labels (shuffled control) before training and following the same analytical procedure.

We ran separate decoders on the neural population to readout information about one of four different variable groups: 1. The current behavior of the animal; 2. Paired vs alone contexts; 3. Neighbor identity when the animals were paired (1-3 in **Fig 3E-F**) and 4. Reciprocity and time elapsed in the session measured during grooming; 5. Time elapsed in the session during rest (4-5 in **Fig S4F**). We used a temporal resolution of 1 second for each decoder.

10. Unsupervised dimensionality reduction of neural population responses (UMAP)

We can treat the activity of a population of simultaneously recorded neurons as a multi-dimensional space where each dimension corresponds to the activity of an individual neuron. A single point in this space therefore would correspond to a particular pattern of neural activity across the entire population and is typically called the neural population state, or neural state for short. There can be meaningful structure in the collection of neural states observed throughout a recording session, and we can look for such structure by visualizing the data with dimensionality reduction methods [80]. We chose to use the state-of-the-art, non-linear dimensionality reduction technique UMAP (Uniform Manifold Approximation and Projection, [40]) to see whether meaningful structure was present within our data. UMAP attempts to retain both the global and local structure of the data, such that the overall "shape" of the data is preserved (global structure) and points that were close in the original space tend to remain close in the dimensionality-reduced space (local structure). We used the firing rates in Hz of all simultaneously recorded units during each behavior as observations (excluding rest and rare behaviors) and reduced the data down to three dimensions. We used the matlab implementation of UMAP toolbox [81], with

parameters: 'n_neighbors'=15, 'min_dist'=0.1, 'n_components'=3. We note that UMAP can be used as a supervised dimensionality reduction technique, but we chose to use the unsupervised variant. This choice ensured that the structure UMAP found was solely due to patterns in the neural states irrespective of information about the current behavior. We plotted the neural states on the first 3 UMAP dimensions and ***post-hoc*** color-coded data points according to what the subject monkey's current behavior was at that time point (**Fig 3A,B**) or the social context (**Fig 3C,D**). We tried multiple parameter configurations and obtained qualitatively similar results (**Fig S3 E-H**).

We also visualized population activity only considering grooming seconds (**Fig 4K** top panels) or rest seconds (**Fig 4K** bottom panels). Post-hoc, we color-coded each data point by the groom or rest bout number that second belongs to.

11. Calculating distance between neural responses

We can quantify how differently a neural population represents one particular behavioral state or context versus another by comparing the patterns of population activity during each behavioral state/context. One way to perform this analysis is to calculate the pairwise Euclidean distance between the observed neural states (see previous section for detailed definition) for each pair of behavioral states/contexts. Unfortunately, using Euclidean distance can yield surprisingly uninterpretable results in a high dimensional space. In brief, it has been previously shown that using Euclidean distance to calculate the nearest neighbor to a query point in a high dimensional space (i.e., >30 dimensions [82,83] can yield the paradoxical result that all data points are equally close or far to the query point (i.e. many/all points are nearest neighbors). We recorded on average 300 units per session and were concerned that we would encounter this dimensionality issue if we used Euclidean distance in the original firing rate space. To mitigate this problem, we first reduced the dimensionality of our data with UMAP (see previous section for more details), an algorithm designed to preserve both local and global structure in the data as much as possible, and then calculated the pairwise Euclidean distance between neural states in this reduced space. We measured distances between neural states (a) across behaviors controlling for the effect of social context (**Fig S3C**); (b) across social contexts controlling for the effect of behavior (**Fig S3D**); (c) during a threat event compared to a baseline state of 'rest' (**Fig 5C**).

a. Distance between behavioral states, controlling for social context

To quantify clustering in UMAP space across all sessions, we measured the average distance within and between behavior across all sessions. To do so, we first reduced the dimensionality of the full session's neural data to 20 dimensions using UMAP ('n_neighbors', 15, 'min_dist', 0.1, 'n_components'=20). Then, we measured the Euclidean distance between neural states of different behaviors using the matlab function pdist. For a given session, we subsampled down to 30 time points per behavior and calculated the distance matrix for these points. We repeated this subsampling procedure 500 times and averaged the distance matrix across all subsamples. To compare activity across sessions, we computed the mean distance between neural states within and across behavioral categories during one social context, the female neighbor block (**Fig S3C** is averaged across all sessions). To measure how similar neural population activity patterns were to "threat to subject" (**Fig 5D**), we computed similarity score $1/1+d(p_i,p_j)$, where $d(p_i,p_j)$ is the mean Euclidean distance between two states p_i and p_j. These results were qualitatively the same irrespective of the number of UMAP dimensions used (n_components=3, 20 or 50). Finally, we also computed a "representational similarity index" comparing population responses to threat to the subject monkey or his partner. Finally, we calculated "Representational similarity" score which is simply the correlation coefficient between the average neural population responses during threat to subject compared to threat to its partner while paired.

b. Distance between social contexts, controlling for behaviors

We used a similar approach than described above to measure distances between states from different social contexts, this time subsampling 100 time points during 'rest' across all three contexts (i.e., alone, paired with female neighbor, paired with male neighbor).

c. Distance between a threatened and a baseline state when paired vs. alone

We considered a baseline state to be the center of mass (i.e., the mean) of all 'rest' neural population states. For each human threats towards the subject, which lasted 30 seconds, we extracted a 90sec window: from 30 seconds before threat onset to 60 seconds after. For each second in that window, we computed the Euclidean distance to baseline in UMAP space. We then split threats towards the subject which occurred when the subject was alone to those where he was paired with his female partner. We normalized distances to 20sec prior to threat onset and plotted this normalized distance to baseline in neural firing space in both conditions (**Fig 5C**, lines are mean and shaded areas are SEM).

12. Addressing movement and field of view potential confounds

Allowing animals to move freely enables the expression of natural behaviors but reduces control over visual inputs and motor outputs. Accordingly, we tested whether our results were merely due to the visuomotor experience of the animal rather than their current behavioral state and social contexts. To do so, we ran a series of complementary analyses (note that all analyses in this section excluded timepoints with missing video tracking data). First, we quantified variation in movement patterns and field of view (FOV) within and across behaviors. Second, we measured explained variance in neural activity by movements and FOV compared to behavioral state. Third, we regressed-out movements and FOV and assessed the effect on decoding accuracy of behavioral state. We discuss each analysis in detail in the following subsections:

a. Preprocessing: aligning video and neural data

We extracted all movement and FOV-related variables from the video data (see video tracking section for more details). For all analyses, we resampled the neural data at 29.97Hz, to match the videos' temporal resolution. We then aligned neural activity with the onset of video recordings. The neural recording system was always started first and stopped last, such that we timestamped when the cameras turned ON and OFF using the same clock as the neural data. We simply trimmed neural activity which occurred before the cameras were started and after they were turned off. These two pre-processing steps allowed the alignment of movement, FOV, behavioral and neural data required for subsequent analyses.

a. Approach 1: Quantifying variability in animal position, movement and field of view within and across behaviors

Across all N=12 sessions, we tested whether there was variation in the visual input of the animal across different instances of a given behavior, and whether similar sensory inputs could occur during different behaviors. This was done to demonstrate a potential dissociation/decorrelation between behavior and visual input. As a proxy for field of view (FOV), we calculated the head direction of the animal based on automatic tracking of the neuro-logger position in videos (see above for method). We plotted the distribution of FOV during four different example behaviors to show that visual input varies extensively during the performance of a single behavior, ruling out that the neural signature of a given behavior is entirely explained by a specific visual input (**Fig 6C**). The overlapping distributions of FOV also demonstrate that visual input can be similar across different behaviors, further dissociating visual input from the neural signature of individual behaviors. In addition to overlap in field of view, we find similar kinematics across two neurally distinct behaviors, self-grooming and allo-grooming (**Fig 3A-B**). After quantifying macaque movement with the HRNet pose tracking model (see previous section on video tracking), we isolated the shoulder, elbow, and wrist 2D trajectories of the subject. We then computed the change in shoulder-elbow-wrist joint angle during two 2-min bouts of self- and allo-grooming (**Fig 6B**).

Second, we tested whether the FOV was similar or different during the 3 tested social contexts. If FOV was different across contexts, it could indicate a potential confound between the neural signatures of social context and visual input. We plotted the distribution of FOV across the three contexts on the same axes (**Fig 6D**). FOV varies widely during a given social context and overlaps almost completely between social contexts, ruling out that a correlation between visual input and context explains all of the contextual neural signatures observed in both monkeys.

b. Approach 2: Measuring relative variance explained by movement and field of view compared to behavior

Next, we ran a multilinear ridge regression analysis to determine how much of the neural variance of each recorded unit could be uniquely explained by the current behavioral state of the animal vs. the sensorimotor environment (**Fig 6E**). The smoothed firing rate for each unit throughout the session was used as the response variable, and the behavioral labels and visuo-motor measurements were used as predictors (see **Appendix 3** for a full description). This method closely replicates the one used in Musall et al. 2019 [51] and Tremblay et al. 2022 [32] to dissociate the neural variance explained by task variables and movement variables. We used 10 sessions for this analysis, 2/12 had to be excluded due to missing side view videos used for pose-tracking (see above for more details).

Predictors could be associated with multiple regressors in the analysis and were labeled as either analog predictors or event predictors (**Fig. S6**). Event predictors had distinct onsets and offsets and could be represented in the model by a regressor that takes on value of 1 when the predictor was occurring and 0 when the predictor was absent (e.g., the foraging behavioral state). To account for preemptive or lagged neural responses, we constructed "event kernels" for each event predictor. Event kernels were comprised of a set of regressors each of which represented a particular delay from the event onset. We included delays from one second before to one second after event onset. It can be useful to think of event kernels as related to the more familiar peri-stimulus time histogram (PSTH). That is, imagine each delay regressor corresponds to one bin of the PSTH; thus, the entire set of delay regressors allows the model to fit a PSTH to each event predictor. Analog predictors, by contrast, took on continuous values throughout the session and could be represented in the model by a regressor that tracks the measured value (e.g., current head position). We noted that it was possible that neuronal responses corresponded with certain analog predictors crossing particular thresholds rather than corresponding with the exact value of that predictor, and, furthermore, that the responses to these threshold crossing could be preemptive or lagged. For example, a neuron could increase its firing in some stereotyped way before an animal initiates a large arm movement. To account for such responses, we created event kernels for the relevant analog predictors. We used a threshold of two standard deviations to determine what qualified as a significant threshold crossing event for an analog predictor and constructed the event kernel as above. We collected all of the regressors resulting from the above processes into an *Observation* X *Regressors* matrix while keeping track of which sets of regressors were associated with which predictors. This matrix was used to fit a linear model with ridge regression regularization in all subsequent analyses.

To determine the proportion of variance explained by each predictor, we used a 10-fold shuffled, hold-out cross-validation procedure to obtain the predicted neural activity by the linear model for each recorded unit individually. We then calculated the correlation between the predicted neural activity and the actual recorded neural activity for all neurons recorded during a session, yielding a single, overall R^2 for the neural population. This R^2 value gave us an estimate of the variance explained by our model when using all possible predictors. To compute the variance explained by a particular predictor group (e.g. Movements), we refit the model but shuffled all other predictors except the predictor of interest, which we called the "Full contribution" model. The explained variance by each "Full contribution model shows the maximum potential predictive power of the predictor of interest (e.g. Behavior ID). To measure each predictor's *unique* contribution to the model, we instead only shuffled the predictor of interest and kept all other predictors as they were, which we called the "unique contribution" model. The difference in explained variance between the model using all predictors and this model yielded the *Unique contribution* (ΔR^2) of that predictor. The unique contribution shows the amount of explained variance in the full model that can be uniquely attributed to the group of model variables associated with that predictor (i.e. nonredundant to all other predictors). To account the potential of overfitting we included a ridge regularization penalty in the regression model. Briefly, ridge regularization effectively sets a limit on the sum of the squared regression coefficients which in turn drives regressors that are not contributing much to model predictions toward, but not to, zero. The strength of this regularization is determined by a scaling parameter called lambda. In our

analyses lambda was set by cross-validation before the model was fit and the same lambda was used for the full and unique contribution model. Again, for more details, see Tremblay, Testard, *et al.* 2022 as well as Musall *et al.* 2019 [51].

c. Approach 3: Regressing out variance explained by movement and field of view for decoding

To further investigate whether neural activity patterns were merely explained by the immediate sensorimotor environment, we re-ran our decoding analyses of the behavioral ethogram after removing neural variance explained by movement and field of view (**Fig 6F**). To do so, we ran a multilinear regression with neural activity as a response variable and sensorimotor variables as predictors, and used the raw residuals of this regression as input to downstream analyses (see Methods section on decoding above for more details). Residuals of this regression correspond to movement and FOV-controlled residual neural activity and the decoding was run on these residuals. We also ran a version of the decoder where residuals from a regression run between neural activity and behavior ID were used. This decoder effectively attempts to decode behavioral states from visual and movement inputs alone. Since behaviors are largely defined by stereotypical movement patterns, decoding accuracy for behavioral state did not fall to chance, as expected. These two decoding analyses allowed to measure the information content of the neural population activity about behavioral state, irrespective of visuomotor confounds.

13. <u>Predicting reciprocity from neural population activity using ridge regression</u>

To investigate whether neural population activity in TEO and vlPFC tracked how reciprocal grooming interactions were at any given second in a session, we used multi-linear ridge regression analysis (same approach as above). We tested how the neural population activity predicted two reciprocity metrics and Time (i.e. response variables, see cartoon in **Fig 4G**): (1) net groom duration (Groom duration received - duration given) and (2) net number of groom bouts (Groom bouts received - bouts given) (3) Time, a continuously monotonically increasing variable. Predictors were the neural population activity (i.e. Time (s) x Neuron matrix). Both predictor and response variables were z-scored. We focused our analysis, first, on grooming time points exclusively, where we were most likely to predict grooming reciprocity from the neural activity. Grooming bouts which occurred for 5 sec or less were excluded from this analysis.

To determine model fit, we used a 5-fold hold-out cross-validation procedure to obtain the predicted reciprocity metric by the linear model from the whole neural population. Note that each fold corresponded to a continuous chunk of data in the session, rather than random sampling of indices within the session, which can lead to overfitting. We then calculated the correlation between the predicted reciprocity metric and the actual metric during a session, yielding an overall R^2. This R^2 value gave us an estimate of the variance explained by our model when using all simultaneously recorded neurons (**Fig 4H**). To investigate whether any given single neuron activity tracked reciprocity, we repeated the aforementioned analysis but for each neuron individually (**Fig S4**). Finally, we asked how well elapsed time could be predicted from the neural activity outside of grooming. We repeated the ridge regression analysis described above but now only including data from non-grooming time points (**Fig 4J**).

SUPPLEMENTARY INFORMATION

Supplementary Figures:

Figure S1. Neural data quality and transitions between behaviors

Figure S2: Single neuron responses to current behavior

Figure S3: Population responses to current behavior and context

FigureS4: Grooming reciprocity

Figure S5: Buffering of neural response to threat

Figure S6: Video tracking

List of Appendices:

1. Cayo ethogram, basis for the experiment's ethogram
2. Comparison of Cayo and Lab ethogram
3. Ethogram (description of behaviors, grooming contexts, visuomotor variables)
4. Intervention description and schedule

Supplementary Movies:

1. Movies S1-4: Example clips of natural behavior in the lab
2. Movies S4-8: Full body tracking certainty cut-off 0.2
3. Movie S9: Logger tracking at 0.8 cutoff.

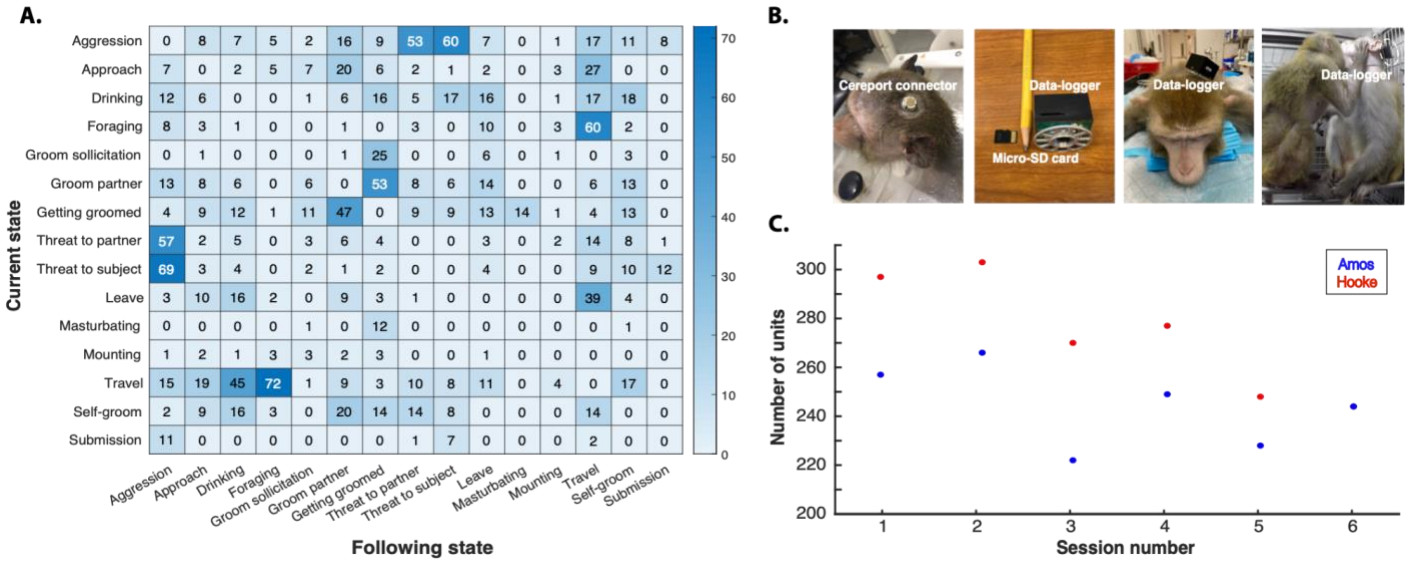

Fig S1. Behavior transition matrix, Neurotechnology and stability of neural data quality. (A) Absolute number of transitions from one behavior to the next across all sessions, monkeys pooled. (B) Images of wireless neural recording device. (C) Number of units recorded across vlPFC and TEO in our two subject monkeys

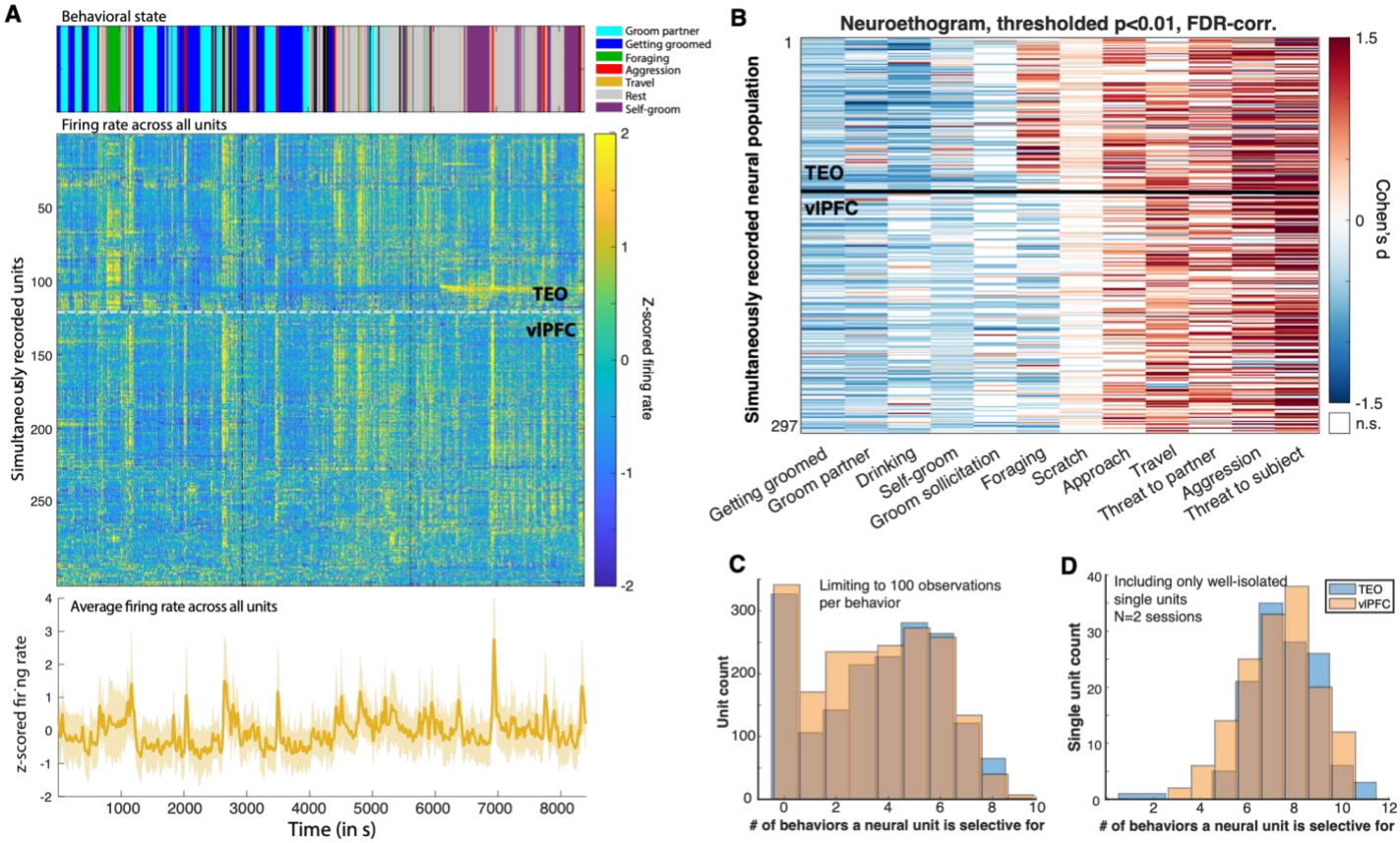

Fig S2. Single unit responses during behavior. (A) Top: behavior during example session; Middle: Z-scored firing rate of all units recorded in the same example session as Fig 2, ordered by activity pattern and units ordered using Rastermap [84]; Bottom: Average z-scored firing across all recorded units in the same session. Shaded area is the standard deviation. (B) Neuro-ethogram from Fig 2D statistically thresholded at FDR-corrected $P < 0.01$. (C) Number of behaviors a neuron is selective for if limiting to 100 observations per behavior (sub-sampling 100 times through the data). (D) Same as Fig 2F but for well-isolated single units only for two sessions (one in each monkey).

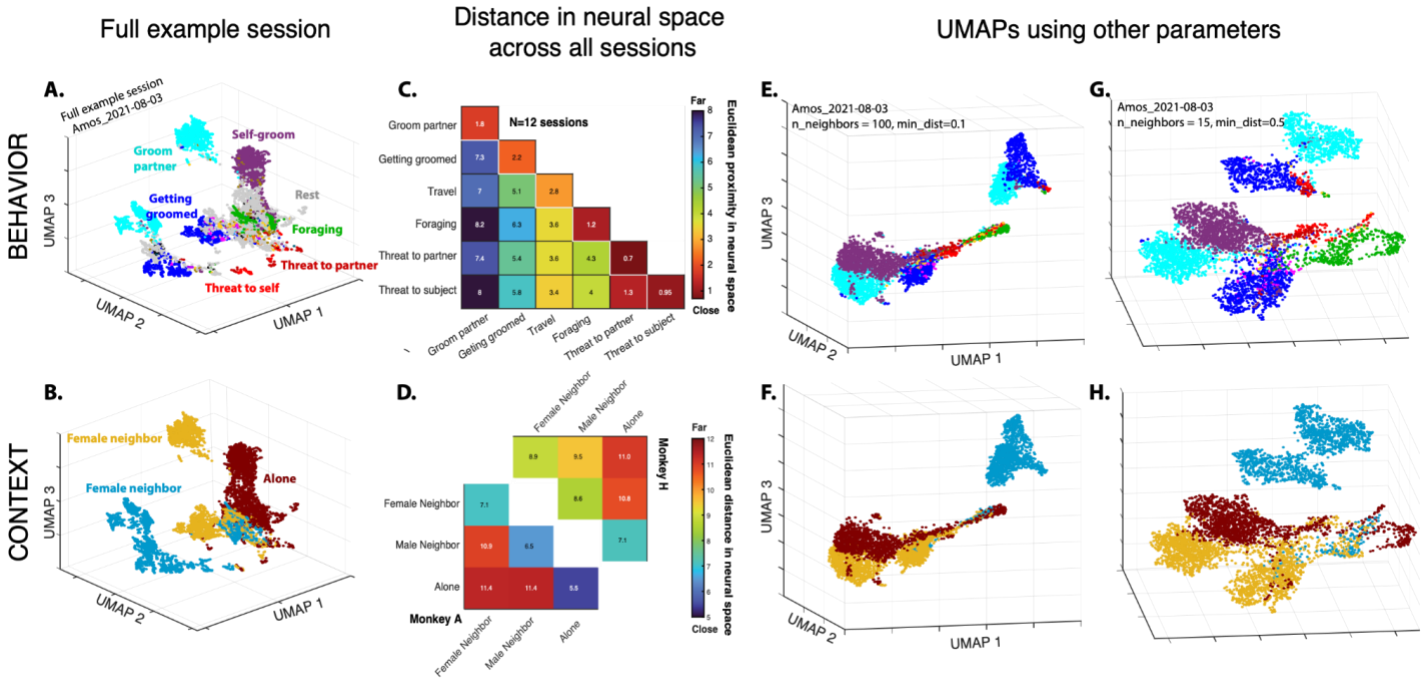

Fig S3. Neural population states separate by behavior and context across sessions. (A-B) Whole session UMAP visualization (same session as in **Fig 2A-D**). (C) Average distance between neural states across behaviors in UMAP space. Pooled across sessions and monkeys. (D) Average distance between neural states across social contexts. (E-H) UMAP plots as in Fig 2A but with different parameter values. Results remain qualitatively the same.

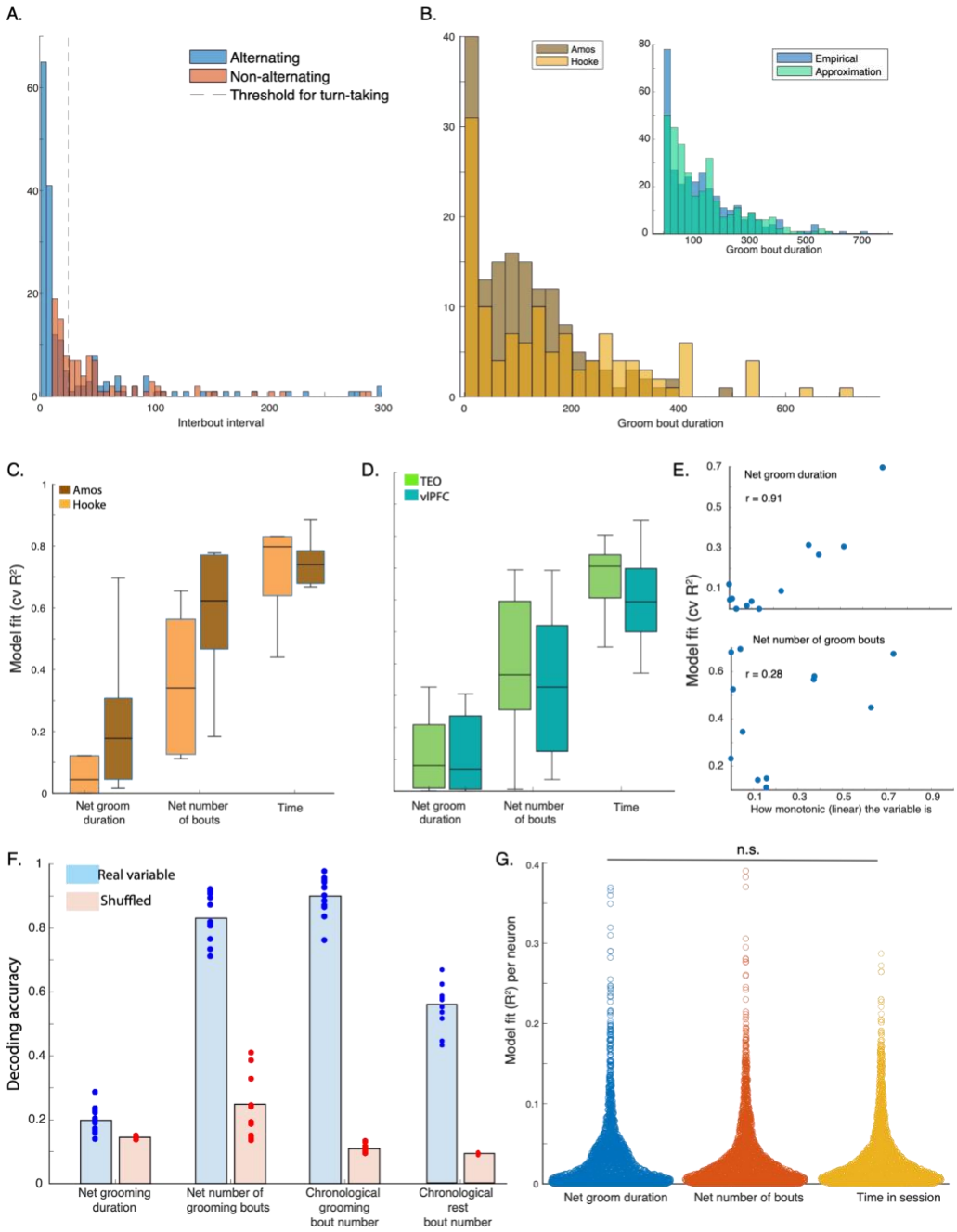

Fig S4. Behavioral evidence for grooming reciprocity and underlying neural mechanisms. (A) Interbout interval for alternating grooming bouts (Give-Receive-Give, blue) vs non-alternating (Give-Give or Receive-Receive, red). Alternating bouts showed a bi-modal distribution with short inter-bout intervals <20s and longer ones. Based on this distribution we considered alternating bouts spaced by less than 20s to be "Turn-taking". (B) Distribution of grooming bout duration for Amos (brown) vs. Hooke (yellow). Inset: Empirical distribution of grooming bout durations (blue) and approximated distribution (turquoise). Approximation uses an exponential distribution with empirical mean bout length as a parameter. (C) Ridge regression model fit (cross-validated R^2) for net grooming duration, net number of bouts and time combining separated by monkey (brain areas pooled). (D) Ridge regression model fit (cross-validated R^2) for net grooming duration, net number of bouts and time combining separated by brain areas (monkeys pooled). (E) Correlation between ridge regression model fit and how linear & monotonic the response variable is. Top: Net groom duration; Bottom: Net number of grooming bouts. (F) Cross-validation (5-fold) linear decoding accuracy of (from left to right): categorical net groom duration, categorical net number of bouts, chronological grooming bout number, chronological rest bout number. Red: shuffled control. (G) Distribution of single neuron cross-validated ridge regression fit for net groom duration, net groom bouts and time. Distributions are not statistically distinguishable.

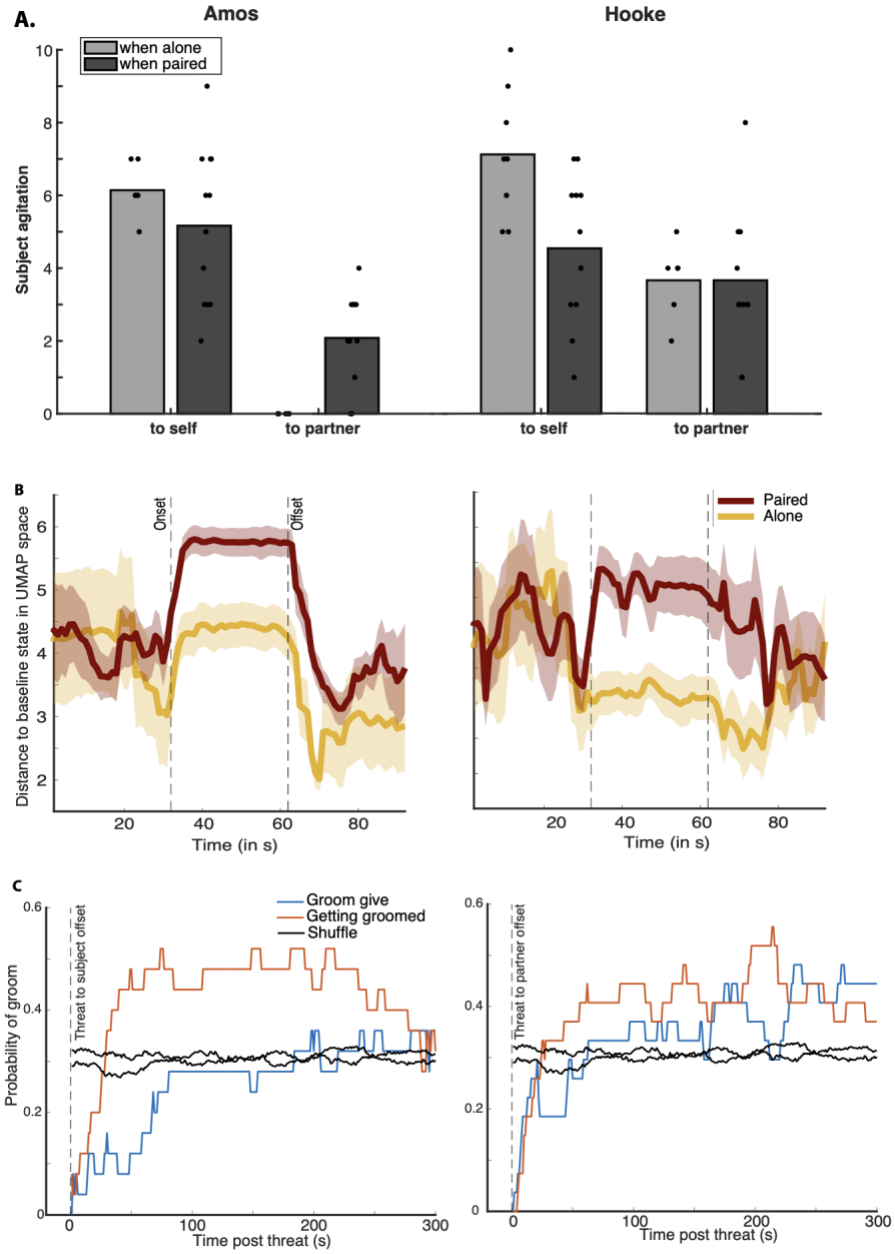

Fig S5. Neural signatures of social support and empathy in response to human threats. (A) Agitation score in response to human threats as in Fig 5B separated by monkey. (B) Same as in Fig 4C separated by monkey. (C) Probability of grooming given or received in the 5min following a threat.

A.

Task	Monkey Detection	Monkey Pose Estimation	Logger Pose Estimation
Library	mmdetection [65]	mmpose [66]	DeepLabCut [73,74]
Model Architecture	Faster-RCNN [68]	HRNet [67,69-70]	ResNet50 [73]
Num. of training images	3,082	4,889	6,486
Num. of instances	3,962	6,084	2,423
Mean average precision (mAP)	99.40%	93.20%	N/A
Mean average error (MAE)	N/A	N/A	5.54 px

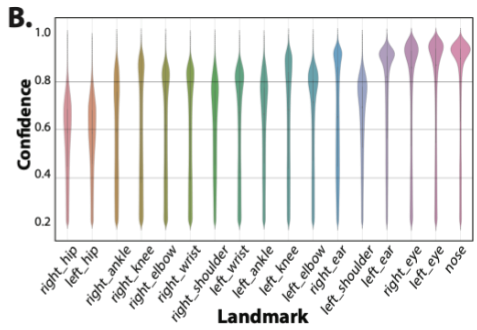

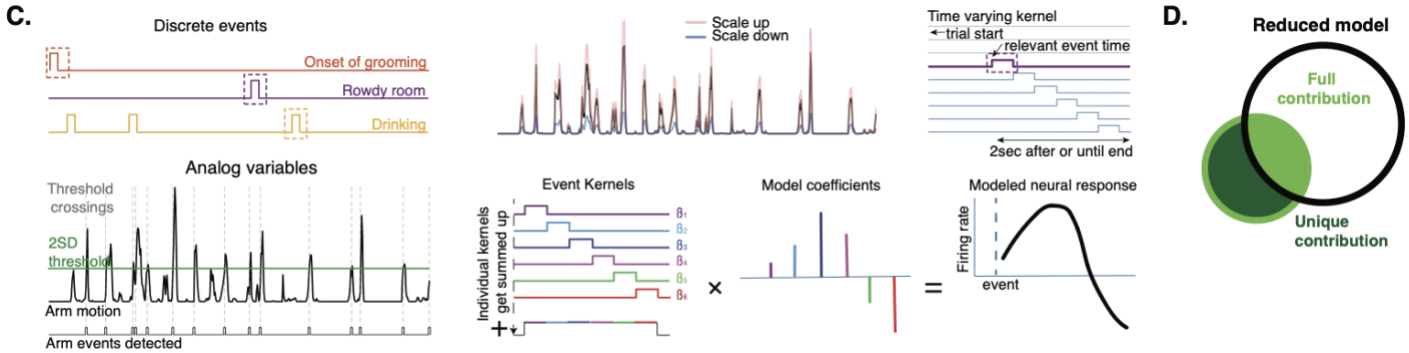

Fig S6. Video-based quantification of behavior. A) Table summarizing behavior quantification models and their accuracies for monkey detection, monkey pose estimation, and logger pose estimation. B) Confidence score by body landmark thresholding at c = 0.2. C-D: Details of ridge regression model to test the relative importance of behavior vs. movements and field of view to explain neural variance (Fig 6). C) Discrete behavior and movement events and analog, continuous variables are included in a linear encoding model (ridge regression). Time-shifted copies of discrete events are created to account for delayed neural responses. A coefficient is estimated for each time-varying event kernels to model neural responses to events on a single-trial basis. D) The contribution of each variable to the model is divided into its total contribution (light green), which may have a redundancy with other model variables, and its unique contribution (dark green) that excludes potential redundancy.

Citation	Species, brain region(s)	Task, analysis of firing	Reported Neural Tuning	Max # , mode # of variables tuned to
Gofman et al. 2019	Mouse - V2, POR, dPrS, PaS, MEC	Free exploration of an enclosed environment - GLM model	Head direction, speed, position, egocentric boundary position.	4, 1
Hardcastle et al. 2017	Mouse - MEC	Free exploration of an enclosed environment - GLM	Position, head direction, speed	3, 2
Rust and Dicarlo 2012	Macaque - V4, IT	Presentation of natural images - Fraction of images causing >50% of peak firing rate response	Response to image from set of 300 natural images	225, 1
Tsao et al. 2018	Mouse - LEC, CA3, MEC	Free exploration of an enclosed environment - GLM	Wall color, position, and time	3, 1
Mao et al. 2020	Macaque - HPC, EC, SUB	Free exploration of an enclosed environment - GLM	Position, facing location, egocentric boundary, head tilt, angular velocity, head height, translational speed, azimuth head direction	Not reported, 2+
Zhang et al. 1997	Macaque - M1	Associative learning pointing task - locus analysis + differential activity peak analysis	Stimulus content, response content, SR rule, SR conjunction	2, 1
Lowe et al. 2022	Macaque - FEF, F2vr	Memory guided saccade + T/L search - Activity peak + consensus clustering algorithm	Visual, visuomovement, movement, functional role in task (clustering analysis)	2, 1
Lanzilotto et al. 2016	Macaque - F6	Grasping and holding task - peak activity	Visual, visuomotor, motor, object held	4, 1

Table S1. Selective literature review on sparse coding from neurophysiological data collected in traditional laboratory settings.

REFERENCES

1. Miller, C. T. *et al.* Natural behavior is the language of the brain. *Curr. Biol.* **32**, R482–R493 (2022).
2. Maestripieri, D. & Hoffman, C. L. Behavior and social dynamics of rhesus macaques on Cayo Santiago. in *Bones, Genetics, and Behavior of Rhesus Macaques: Macaca Mulatta of Cayo Santiago and Beyond* (ed. Wang, Q.) 247–262 (Springer, 2012).
3. Snyder-Mackler, N. *et al.* Social determinants of health and survival in humans and other animals. *Science* (2020) doi:10.1126/science.aax9553.
4. Silk, J. B. Social components of fitness in primate groups. *Science* **317**, 1347–1351 (2007).
5. Testard, C. *et al.* Rhesus macaques build new social connections after a natural disaster. *Curr. Biol.* **31**, 2299–2309.e7 (2021).
6. Holt-Lunstad, J., Smith, T. B. & Layton, J. B. Social relationships and mortality risk: a meta-analytic review. *PLoS Med.* **7**, e1000316 (2010).
7. Holt-Lunstad, J., Robles, T. F. & Sbarra, D. A. Advancing social connection as a public health priority in the United States. *Am. Psychol.* **72**, 517–530 (2017).
8. Sterling, P. & Platt, M. L. Why deaths of despair are increasing in the US and not other industrial nations—insights from neuroscience and anthropology. *JAMA Psychiatry* (2022).
9. Watson, K. K. & Platt, M. L. Social signals in primate orbitofrontal cortex. *Curr. Biol.* (2012).
10. Klein, J. T. & Platt, M. L. Social information signaling by neurons in primate striatum. *Curr. Biol.* (2013).
11. Chang, S. W. C., Gariépy, J.-F. & Platt, M. L. Neuronal reference frames for social decisions in primate frontal cortex. *Nat. Neurosci.* **16**, 243–250 (2013).
12. Bonini, L., Maranesi, M., Livi, A., Fogassi, L. & Rizzolatti, G. Ventral premotor neurons encoding representations of action during self and others' inaction. *Curr. Biol.* (2014).
13. Ballesta, S. & Duhamel, J.-R. Rudimentary empathy in macaques' social decision-making. *Proc. Natl. Acad. Sci. U. S. A.* **112**, 15516–15521 (2015).
14. Haroush, K. & Williams, Z. M. Neuronal prediction of opponent's behavior during cooperative social interchange in primates. *Cell* **160**, 1233–1245 (2015).
15. Ong, W. S., Madlon-Kay, S. & Platt, M. L. Neuronal correlates of strategic cooperation in monkeys. *Nat. Neurosci.* (2020) doi:10.1038/s41593-020-00746-9.
16. Dal Monte, O. *et al.* Widespread implementations of interactive social gaze neurons in the primate prefrontal-amygdala networks. *Neuron* **110**, 2183–2197.e7 (2022).
17. Testard, C., Tremblay, S. & Platt, M. From the field to the lab and back: neuroethology of primate social behavior. *Curr. Opin. Neurobiol.* **68**, 76–83 (2021).
18. Cooper, E. B. *et al.* The rhesus macaque as a success story of the Anthropocene. *Elife* **11**, e78169 (2022).
19. Dubuc, C., Hughes, K. D., Cascio, J. & Santos, L. R. Social tolerance in a despotic primate: co-feeding between consortship partners in rhesus macaques. *Am. J. Phys. Anthropol.* **148**, 73–80 (2012).
20. Schino, G. Grooming and agonistic support: A meta-analysis of primate reciprocal altruism. *Behav. Ecol.* **18**, 115–120 (2007).
21. Aparicio, P. L., Issa, E. B. & DiCarlo, J. J. Neurophysiological Organization of the Middle Face Patch in Macaque Inferior Temporal Cortex. *J. Neurosci.* **36**, 12729–12745 (2016).
22. Bizley, J. K. & Cohen, Y. E. The what, where and how of auditory-object perception. *Nat. Rev. Neurosci.* (2013).
23. Sliwa, J. & Freiwald, W. A. A dedicated network for social interaction processing in the primate brain. *Science* **356**, 745–749 (2017).
24. Kravitz, D. J., Saleem, K. S., Baker, C. I., Ungerleider, L. G. & Mishkin, M. The ventral visual pathway: an expanded neural framework for the processing of object quality. *Trends Cogn. Sci.* **17**, 26–49 (2013).
25. Sugihara, T., Diltz, M. D., Averbeck, B. B. & Romanski, L. M. Integration of auditory and visual communication information in the primate ventrolateral prefrontal cortex. *J. Neurosci.* **26**, 11138–11147 (2006).
26. Passingham, R. E. & Wise, S. P. *The neurobiology of the prefrontal cortex : anatomy, evolution, and the*

origin of insight. (Oxford University Press, 2014).
27. Boussaoud, D., Desimone, R. & Ungerleider, L. G. Visual topography of area TEO in the macaque. *J. Comp. Neurol.* **306**, 554–575 (1991).
28. Setogawa, T., Eldridge, M. A. G., Fomani, G. P., Saunders, R. C. & Richmond, B. J. Contributions of the Monkey Inferior Temporal Areas TE and TEO to Visual Categorization. *Cereb. Cortex* **31**, 4891–4900 (2021).
29. Felleman, D. J. & Van Essen, D. C. Distributed hierarchical processing in the primate cerebral cortex. *Cereb. Cortex* **1**, 1–47 (1991).
30. Rigotti, M. *et al.* The importance of mixed selectivity in complex cognitive tasks. *Nature* **497**, 585–590 (2013).
31. Gofman, X. *et al.* Dissociation between Postrhinal Cortex and Downstream Parahippocampal Regions in the Representation of Egocentric Boundaries. *Curr. Biol.* **29**, 2751–2757.e4 (2019).
32. Tremblay, S., Testard, C., DiTullio, R. W., Inchauspé, J. & Petrides, M. Neural cognitive signals during spontaneous movements in the macaque. *Nat. Neurosci.* (2022) doi:10.1038/s41593-022-01220-4.
33. Rust, N. C. & DiCarlo, J. J. Balanced increases in selectivity and tolerance produce constant sparseness along the ventral visual stream. *J. Neurosci.* **32**, 10170–10182 (2012).
34. Beyeler, M., Rounds, E. L., Carlson, K. D., Dutt, N. & Krichmar, J. L. Neural correlates of sparse coding and dimensionality reduction. *PLoS Comput. Biol.* **15**, e1006908 (2019).
35. Laughlin, S. B. Energy as a constraint on the coding and processing of sensory information. *Curr. Opin. Neurobiol.* **11**, 475–480 (2001).
36. Levy, W. B. & Baxter, R. A. Energy efficient neural codes. *Neural Comput.* **8**, 531–543 (1996).
37. Niven, J. E. & Laughlin, S. B. Energy limitation as a selective pressure on the evolution of sensory systems. *J. Exp. Biol.* **211**, 1792–1804 (2008).
38. Quian Quiroga, R. & Panzeri, S. Extracting information from neuronal populations: information theory and decoding approaches. *Nat. Rev. Neurosci.* **10**, 173–185 (2009).
39. Murray, J. D. *et al.* Stable population coding for working memory coexists with heterogeneous neural dynamics in prefrontal cortex. *Proceedings of the National Academy of Sciences* **114**, 394–399 (2017).
40. McInnes, L., Healy, J. & Melville, J. UMAP: Uniform Manifold Approximation and Projection for Dimension Reduction. *arXiv [stat.ML]* (2018).
41. Chang, C.-C. & Lin, C.-J. LIBSVM: A library for support vector machines. *ACM Trans. Intell. Syst. Technol.* **2**, 1–27 (2011).
42. Cheney, D., Seyfarth, R. & Smuts, B. Social relationships and social cognition in nonhuman primates. *Science* **234**, 1361–1366 (1986).
43. Marshall, H. H., Carter, A. J., Ashford, A., Rowcliffe, J. M. & Cowlishaw, G. Social effects on foraging behavior and success depend on local environmental conditions. *Ecol. Evol.* **5**, 475–492 (2015).
44. Gintis, H. Strong reciprocity and human sociality. *J. Theor. Biol.* **206**, 169–179 (2000).
45. Gomes, C. M. & Boesch, C. Reciprocity and trades in wild West African chimpanzees. *Behav. Ecol. Sociobiol.* **65**, 2183–2196 (2011).
46. Majolo, B., Schino, G. & Aureli, F. The relative prevalence of direct, indirect and generalized reciprocity in macaque grooming exchanges. *Anim. Behav.* **83**, 763–771 (2012).
47. de Waal, F. B. & Luttrell, L. M. Mechanisms of social reciprocity in three primate species: Symmetrical relationship characteristics or cognition? *Ethology & Sociobiology* **9**, 101–118 (1988).
48. Schino, G., di Sorrentino, E. P. & Tiddi, B. Grooming and coalitions in Japanese macaques (Macaca fuscata): partner choice and the time frame reciprocation. *J. Comp. Psychol.* **121**, 181–188 (2007).
49. Young, C., Majolo, B., Schülke, O. & Ostner, J. Male social bonds and rank predict supporter selection in cooperative aggression in wild Barbary macaques. *Anim. Behav.* **95**, 23–32 (2014).
50. Hinde, R. A. & Rowell, T. E. Communication by postures and facial expressions in the rhesus monkey (Macaca mulatta). *Proc. Zool. Soc. Lond.* **138**, 1–21 (1962).
51. Musall, S., Kaufman, M. T., Juavinett, A. L., Gluf, S. & Churchland, A. K. Single-trial neural dynamics are dominated by richly varied movements. *Nat. Neurosci.* **22**, 1677–1686 (2019).

52. Stringer, C. *et al.* Spontaneous behaviors drive multidimensional, brainwide activity. *Science* **364**, eaav7893 (2019).
53. Tremblay, S., Testard, C., DiTullio, R. W., Inchauspé, J. & Petrides, M. Neural cognitive signals during spontaneous movements in the macaque. *bioRxiv* 2022.09.05.506681 (2022) doi:10.1101/2022.09.05.506681.
54. Niell, C. M. & Stryker, M. P. Modulation of visual responses by behavioral state in mouse visual cortex. *Neuron* **65**, 472–479 (2010).
55. Avitan, L. & Stringer, C. Not so spontaneous: Multi-dimensional representations of behaviors and context in sensory areas. *Neuron* **110**, 3064–3075 (2022).
56. Tremblay, S., Testard, C., Inchauspé, J. & Petrides, M. Non-necessary neural activity in the primate cortex. *bioRxiv* 2022.09.12.506984 (2022) doi:10.1101/2022.09.12.506984.
57. Blackman, R. K. *et al.* Shared Neural Activity But Distinct Neural Dynamics for Cognitive Control in Monkey Prefrontal and Parietal Cortex. *J. Neurosci.* (2023) doi:10.1523/JNEUROSCI.1641-22.2023.
58. Heiligenberg, W. *Neural Nets in Electric Fish*. (MIT Press, 1991).
59. Brent, L. J. N., Chang, S. W. C., Gariépy, J.-F. & Platt, M. L. The neuroethology of friendship. *Ann. N. Y. Acad. Sci.* **1316**, 1–17 (2014).
60. Bergan, J. F., Ro, P., Ro, D. & Knudsen, E. I. Hunting increases adaptive auditory map plasticity in adult barn owls. *J. Neurosci.* **25**, 9816–9820 (2005).
61. Liberti, W. A., 3rd, Schmid, T. A., Forli, A., Snyder, M. & Yartsev, M. M. A stable hippocampal code in freely flying bats. *Nature* **604**, 98–103 (2022).
62. Pearson, J. M., Watson, K. K. & Platt, M. L. Decision making: the neuroethological turn. *Neuron* **82**, 950–965 (2014).

63. Altmann, J. Observational study of behavior: sampling methods. *Behaviour* **49**, 227–267 (1974).
64. Maestripieri, D. & Hoffman, C. L. Behavior and Social Dynamics of Rhesus Macaques on Cayo Santiago. in *Bones, Genetics, and Behavior of Rhesus Macaques: Macaca Mulatta of Cayo Santiago and Beyond* (ed. Wang, Q.) 247–262 (Springer New York, 2012).
65. Cheney, D. L. & Seyfarth, R. M. How monkeys see the world: Inside the mind of another species. (2018).
66. Chen, K. *et al.* MMDetection: Open MMLab Detection Toolbox and Benchmark. *arXiv [cs.CV]* (2019).
67. MMPose Contributors. OpenMMLab Pose Estimation Toolbox and Benchmark. Preprint at https://github.com/open-mmlab/mmpose (2020).
68. Pan, S. J. & Yang, Q. A Survey on Transfer Learning. *IEEE Trans. Knowl. Data Eng.* **22**, 1345–1359 (2010).
69. Labuguen, R. *et al.* MacaquePose: A Novel 'In the Wild' Macaque Monkey Pose Dataset for Markerless Motion Capture. *Front. Behav. Neurosci.* **14**, (2021).
70. Ren, S., He, K., Girshick, R. & Sun, J. Faster R-CNN: Towards Real-Time Object Detection with Region Proposal Networks. in *Advances in Neural Information Processing Systems* (eds. Cortes, C., Lawrence, N., Lee, D., Sugiyama, M. & Garnett, R.) vol. 28 (Curran Associates, Inc., 2015).
71. Sun, K., Xiao, B., Liu, D. & Wang, J. Deep high-resolution representation learning for human pose estimation. in *2019 IEEE/CVF Conference on Computer Vision and Pattern Recognition (CVPR)* 5693–5703 (IEEE, 2019).
72. Yao, Y. *et al.* OpenMonkeyChallenge: Dataset and Benchmark Challenges for Pose Estimation of Non-human Primates. *International Journal of Computer Vision* vol. 131 243–258 Preprint at https://doi.org/10.1007/s11263-022-01698-2 (2023).
73. Dwyer, B., Nelson, J., Solawetz, J., et. al. *Roboflow (Version 1.0) [Software]. Available from https://roboflow.com*. (2022).
74. Pedregosa, F. *et al.* Scikit-learn: Machine Learning in Python. *arXiv [cs.LG]* 2825–2830 (2012).
75. Candan, Ç. & Inan, H. A unified framework for derivation and implementation of Savitzky–Golay filters. *Signal Processing* **104**, 203–211 (2014).
76. Mathis, A. *et al.* DeepLabCut: markerless pose estimation of user-defined body parts with deep learning.

Nat. Neurosci. **21**, 1281–1289 (2018).
77. Nath, T. *et al.* Using DeepLabCut for 3D markerless pose estimation across species and behaviors. *Nat. Protoc.* **14**, 2152–2176 (2019).
78. Benjamini, Y. & Hochberg, Y. Controlling the False Discovery Rate: A Practical and Powerful Approach to Multiple Testing. *J. R. Stat. Soc. Series B Stat. Methodol.* **57**, 289–300 (1995).
79. Groppe, D. *fdr_bh*. (Retrieved March 4 2023).
80. Humphries, M. D. Strong and weak principles of neural dimension reduction. *Neurons, Behavior, Data analysis, and Theory* **5**, (2021).
81. Connor Meehan, Jonathan Ebrahimian, Wayne Moore, and Stephen Meehan. Uniform Manifold Approximation and Projection (UMAP). Preprint at https://www.mathworks.com/matlabcentral/fileexchange/71902 (2022).
82. Aggarwal, C. C., Hinneburg, A. & Keim, D. A. On the Surprising Behavior of Distance Metrics in High Dimensional Space. in *Database Theory — ICDT 2001* 420–434 (Springer Berlin Heidelberg, 2001).
83. Beyer, K., Goldstein, J., Ramakrishnan, R. & Shaft, U. When Is 'Nearest Neighbor' Meaningful? in *Database Theory — ICDT'99* 217–235 (Springer Berlin Heidelberg, 1999).
84. Stringer C., P. M. *Rastermap: unsupervised visualization of high-dimensional neural activity*. (2021).